CARBON FOAM CHARACTERIZATION:

SANDWICH FLEXURE, TENSILE AND SHEAR RESPONSE

A Thesis

by

MELANIE DIANE SARZYNSKI

Submitted to the Office of Graduate Studies of
Texas A&M University
in partial fulfillment of the requirements for the degree of

MASTER OF SCIENCE

December 2003

Major Subject: Mechanical Engineering

CARBON FOAM CHARACTERIZATION:

SANDWICH FLEXURE, TENSILE AND SHEAR RESPONSE

A Thesis

by

MELANIE DIANE SARZYNSKI

Submitted to Texas A&M University
in partial fulfillment of the requirements for the degree of

MASTER OF SCIENCE

Approved as to style and content by:

Ozden Ochoa (Chair of Committee)	Paul Roschke (Member)
Harry Hogan (Member)	Dennis O'Neal (Head of Department)
William Schneider (Member)	

December 2003

Major Subject: Mechanical Engineering

ABSTRACT

Carbon Foam Characterization: Sandwich Flexure,
Tensile and Shear Response. (December 2003)
Melanie Diane Sarzynski, B.S., Texas A&M University
Chair of Advisory Committee: Dr. Ozden Ochoa

The focus of this research is characterizing a new material system composed of carbon and graphite foams, which has potential in a wide variety of applications encompassing aerospace, military, offshore, power production and other commercial industries. The benefits of this new material include low cost, light weight, fire-resistance, good energy absorption, and thermal insulation or conduction as desired. The objective of this research is to explore the bulk material properties and failure modes of the carbon foam through experimental and computational analysis in order to provide a better understanding and assessment of the material for successful design in future applications.

Experiments are conducted according to ASTM standards to determine the mechanical properties and failure modes of the carbon foam. Sandwich beams composed of open cell carbon foam cores and carbon-epoxy laminate face sheets are tested in the flexure condition using a four point setup. The primary failure mode is shear cracks developing in the carbon foam core at a critical axial strain value of 2,262 με. In addition to flexure, the carbon foam is loaded under tensile and shear loads to determine the respective material moduli.

Computational analysis is undertaken to further investigate the carbon foam's failure modes and material characteristics in the sandwich beam configuration. Initial estimates are found using classical laminated plate theory and a linear finite element model. Poor results were obtained due to violation of assumptions used in both cases. Thus, an additional computational analysis

incorporating three dimensional strain-displacement relationships into the finite element analysis is used. Also, a failure behavior pattern for the carbon foam core is included to simulate the unique failure progression of the carbon foam on a microstructure level. Results indicate that displacements, strains and stresses from the flexure experiments are closely predicted by this two parameter progressive damage model. The final computational model consisted of a bond line (interface) study to determine the source of the damage initiation, and it is concluded that damage initiates in the carbon foam, not at the bond line.

TABLE OF CONTENTS

Page

LIST OF FIGURES

FIGURE Page

LIST OF TABLES

1. INTRODUCTION

1.1 Overview

Carbon and graphite foams encompass a brand new material system with potential in a wide variety of applications encompassing aerospace, military, offshore, power production and other commercial industries. The benefits of this new material include low cost, light weight, fire-resistance, good energy absorption, and thermal insulation or conduction as desired [1].

Carbon foams were first developed in the late 1960's by Walter Ford [2,3]. These open cell foams were made by pyrolysis of thermosetting polymer foam to obtain a skeleton of carbon and were named reticulated vitreous carbon (RVC) foam. RVC foams are low cost systems for thermal insulation, impact absorption, and dimensional stability characteristics as required in most aerospace and other industrial applications. In the 1990s, the Air Force Research Laboratory (AFRL) began investigating the production of carbon foam from other precursors such as pitches and coal [2,3]. The resulting microcellular graphitic carbon foam was created by applying a blowing technique to mesophase pitches. More recently, new manufacturing developments have been made at Oakridge National Laboratory (ORNL) [4,5]. Changes in the manufacturing process have led to enhancement of certain thermal properties, and are leading the way to use of carbon foam in multiple thermal management applications.

The graphite foams utilize a pitch-based precursor and are typically heated to a high temperature to modify the structure after the foam is formed. This procedure is also known as graphitization. Carbon foams can use either coal or pitch as the precursor and are not graphitized. The focus of this research is CFOAM, an open cell carbon foam produced by Touchstone Research Laboratory (TRL) from high-sulfur bituminous coal,

---

This thesis follows the style and format of *Journal of Composite Materials*.

which can be obtained for pennies per pound of raw material [1]. After the raw material undergoes preparation, the precursor is foamed at a controlled temperature and pressure. Then, the product can be heat treated to either calicination or graphitization to impart certain characteristics to the final product. Finally, the product undergoes cutting, machining and other finishing operations as required for the specific application [6]. The exact manufacturing process is a patented, proprietary process that is still undergoing modifications and refinement. These carbon and graphite foams are still relatively new, and have only been commercially available for approximately two years. As the material becomes more available to industry, the list of potential applications will continue to grow; however, there are some promising potential applications currently under development.

ORNL is currently investigating and applying the unique thermal properties of graphite foam to fuel cells, advanced power electronic heat sinks, nuclear power plant cores, heat exchangers, and brake/clutch cooling [5]. Combustion-resistance is another key attraction of this material for researchers in both military and commercial applications. For example, carbon and graphite foams do not ignite, and their fire resistance is critical for offshore and naval applications where fires are a special concern [7]. The foams are also undergoing examination for use in thermal protection systems (TPS), radiators, fireproof containers and electrodes.

Other research efforts are focusing on the structural benefits of carbon foam, especially within the aerospace industry, where weight is a concern. Carbon foam alone is very brittle; however, when used as core in a sandwich construction with laminated composite face sheets, it becomes an enabling system for specific strength tailorablity for crash protection especially in racecars and small aircraft applications. Tests have shown that carbon foam performs better than conventional polyurethane foams currently used for impact absorption [7]. The U.S. Navy is currently investigating its use in air intake and ventilation ducts, as "elevator" floor for aircraft carriers and as lightweight ship hulls and other structures [8]. NASA is also evaluating carbon foam by conducting tests aboard the International Space Station to evaluate its use in future space

applications [9]. Other potential applications include support structures for mirrors, EMI and radar-selective shielding, filtration and catalyst beds and noise reduction [6].

The focus of this research is to investigate the sandwich beam configuration to assess the strength and stiffness range in structural applications. Typically, sandwich beams consist of three or more constituents: the face sheets, the core and the adhesive, assuming cold curing is not used [10,11]. Normally, the strong, stiff face sheets are separated by a layer of less-dense material, or core, which has lower strength and stiffness as shown in Figure 1. In this research, carbon-epoxy laminated face sheets are bonded to the carbon foam core with adhesive to form a symmetric sandwich about the core reference axis.

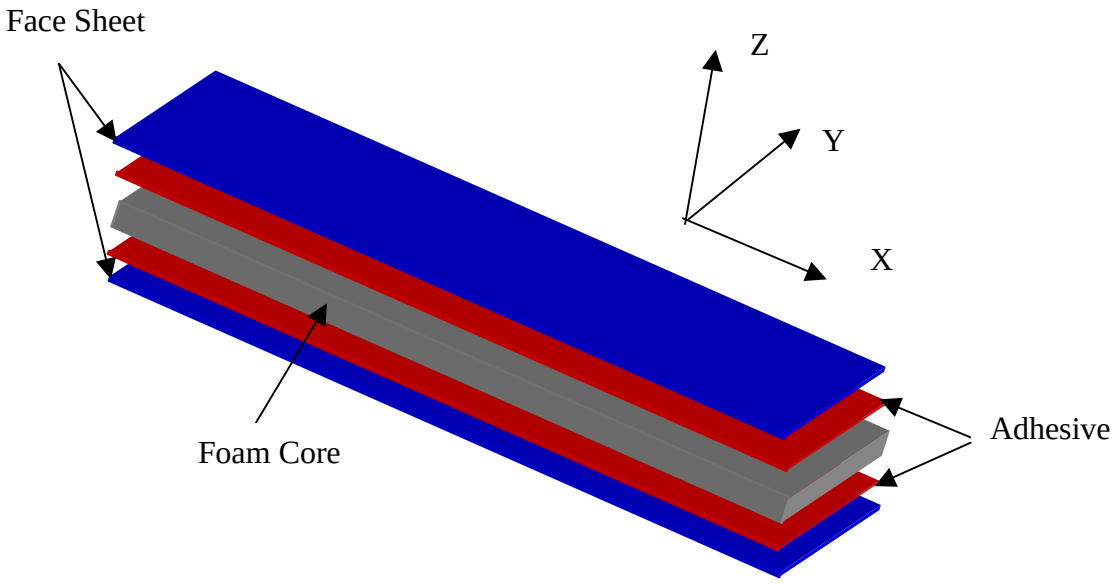

Figure 1. Symmetric sandwich beam construction

In general, sandwich beams offer an increase in the strength of the structure relative to the face sheets alone, while minimizing weight. By separating the stiff face

sheets, the second moment of inertia is increased thus increasing the overall stiffness of the structure with only a minimal increase in weight. They can be loaded in-plane, out-of-plane or in combination depending on the specific application. This results in five basic failure modes—face sheet failure in tension or compression, core failure in shear or compression, failure by general buckling, failure by local buckling, or bond-line failure (delamination at interface) [12]. The face sheets bear most of the in-plane loads as well as any transverse bending stresses, whereas the core serves two main structural functions: it resists deformation perpendicular to the in-plane direction, and provides shear rigidity along the planes perpendicular to the face sheets [10].

1.2 Literature Review

Most studies completed to date on the carbon foam products relate the processing parameters to the microstructure outcome. The carbon foam microstructure produced by AFRL and ORNL, appears to be truss like with a tetrahedral shape as seen in Figure 2. A typical cross section of these foams appears in Figure 3. The ligaments tend to have varying cross sections as well as curvature along the length of the ligament.

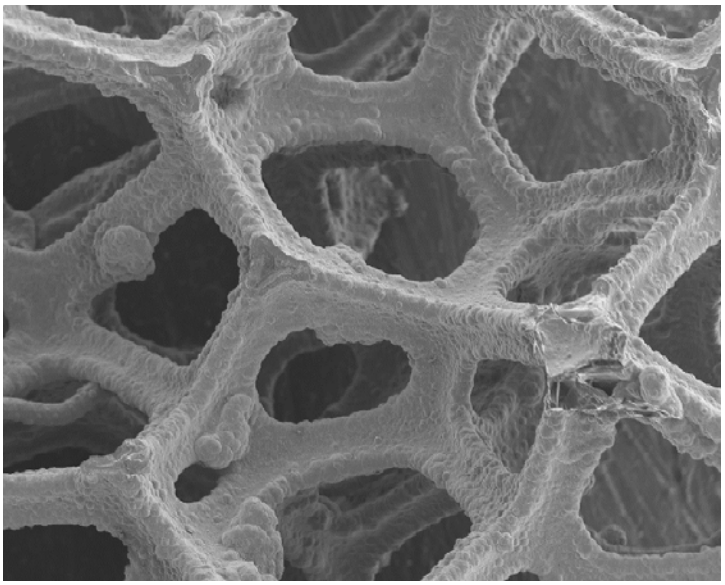

Figure 2. Truss structure formed by ligaments in pitch based carbon foams

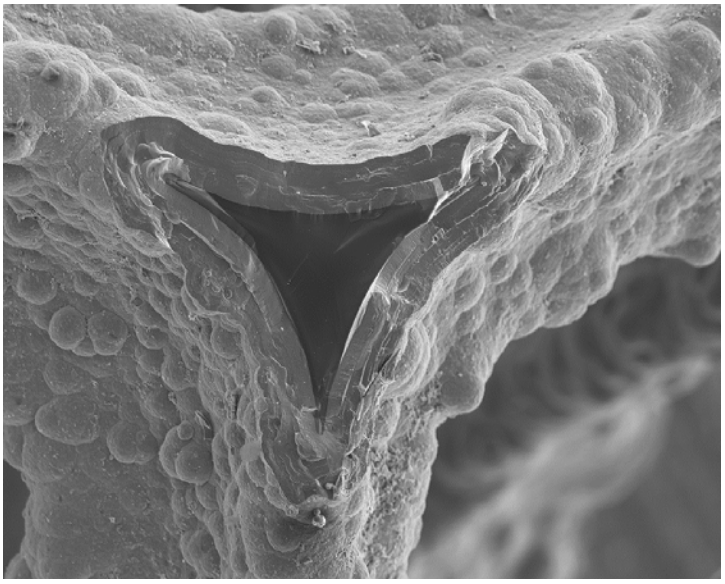

Figure 3. Cross sectional profile of truss ligaments in pitch based carbon foams

Gibson and Ashby have studied cellular solids in great detail [13]. Their work covers honeycomb as well as open and closed cell foams. The focus of this work is on

foams characterized by the truss structure in Figure 2, and the equations developed for traditional foams are used extensively in research to predict mechanical properties of carbon foams with a truss configuration.

Sihn and Roy have modeled the three dimensional microstructure in order to obtain an understanding of the performance of open cell foam materials by correlating microstructural properties to bulk properties [14]. They develop a unit cell that consists of truss representation of ligaments in finite elements to predict the bulk behavior of the foam.

This rationale is expanded to create a spherical unit cell of ligaments (tetrakaidechadral) by Li, Gao and Roy as depicted in Figure 2, where a micromechanics model for three dimensional open cell foams based on energy methods is utilized [2]. A single unit cell is isolated from the carbon foam and used as a representative volume element (RVE). For the RVE, an energy method based on Castigliano's second theorem is applied assuming each ligament to be a slender beam with linearly elastic and isotropic material properties. Unlike previous studies, a parametric study is completed to vary the cross section shape of the ligaments. The model agrees well with closed form formulations in predicting Young's modulus and effective Poisson's ratio.

The carbon foam produced by TRL has a slightly different microstructure as seen in Figure 4. Instead of the well defined truss structure as before, the areas between the ligaments are filled in with more material producing a more solid spherical shaped wall, while still maintaining an open cell characteristic. The cross sections of these ligaments are much different than the above truss ligaments. Instead of having a slender truss structure with length dimensions greater than cross-section dimensions, the ligament is more similar to a thin plate.

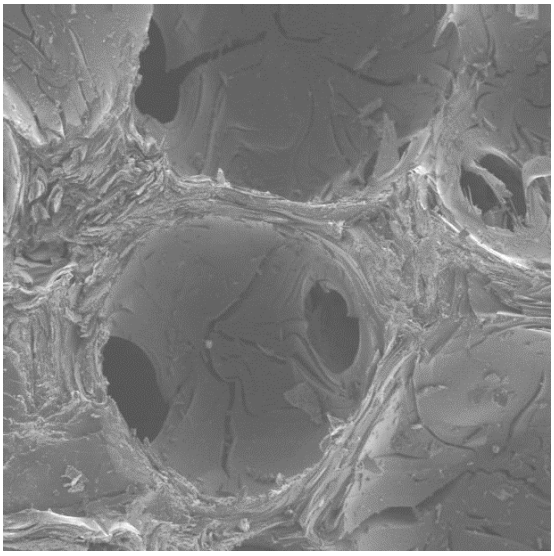

Figure 4. Filled in truss structure in coal based carbon foams [5]

This type of microstructure appears to be a carbon matrix with inhomogeneous inclusions of air. Kanaun and Kochekseraii have used Gaussian approximating functions in the solution of the volume integral equation of thermo- and electro-statics for medium with isolated inhomogeneous inclusions [15]. This work serves to predict the bulk properties, elastic and thermal, based on an analytical model of a representative volume element (RVE).

On the other hand, there has been a wealth of studies on sandwich beams utilizing either honeycomb or tubular core structures of varying material systems other than carbon foam. For example, Meraghni, Desrumaux, and Benzeggragh have studied the mechanical behavior of structural sandwich beams consisting of honeycomb and tubular core types where three different techniques are utilized—a finite element analysis, an analytical study and experimental tests [16]. The results indicate that a higher order analytical model, or a finite element analysis provide the closest results for predicting sandwich rigidities.

Other research has focused on sandwich beams utilizing foam cores, with emphasis placed on polymer foams. Triantafillou and Gibson have developed a failure

mode map for foam core sandwich beams [17]. Equations based on beam theory are developed to predict the load at failure for each possible failure mode that occurs in a sandwich structure consisting of plastically yielding face sheet and core materials. They report that failure indeed can be predicted based on relative core density and ratio of face sheet thickness to span length for a given loading condition.

Dai and Hahn have studied the static and fatigue behavior of vacuum-assisted resin transfer molded sandwich beams under flexural loading [18]. Two core materials, balsa wood and PVC foam, are used to investigate the effects of core material on three and four point flexure tests. This study uses simple beam theory to evaluate the stresses at the face sheets and in the cores to determine the strengths and failure mechanisms of the two cores. A shear dominated failure mode in the core is noted for short beams of both materials. It is also noted that face sheet wrinkling occurs in the PVC foam core due to low modulus in the thickness direction.

The nonlinear flexure response of PVC foam core sandwich beams is the focus for a study undertaken by Sokolinsky, Shen, Vaikhanski and Nutt [19]. The sandwiches studied consist of PVC foam cores with aluminum face sheets. The study compares experimental four point flexure testing to classical sandwich theory, linear and geometrically nonlinear higher-order sandwich beam theory. The results indicate the practical value of using a geometrically nonlinear higher-order theory in predicting the experimental results as over design is likely to be avoided.

The potential weight savings and dimensional tradeoffs are identified by Hall and Hager for applications using truss ligament graphitic foam developed by AFRL in simple, stiffness-critical structural elements [20]. The foam is compared to a refractory alloy, a unidirectional composite, a cross ply composite and commercially available silicon carbide and amorphous carbon foams. The applications studied include plates in flexure and buckling, and beams in flexure and buckling, or tension. The results identify that the graphitic foams can offer improved stiffness that can compete with or improve performance of the comparison materials.

Hall also compares the performance of truss ligament carbon foam core sandwich beams to honeycomb core sandwiches beams that are subjected to cylindrical bending [21]. In addition, three constitutive models are considered to estimate the foam shear modulus and shear deformation. It is noted that as porosity increased the shear deformation increased significantly and higher-order theories should be used for accuracy. The carbon foam cores appear to have higher in-plane and bending stiffnesses in comparison to honeycomb core sandwiches composed of aluminum.

1.3 Objective

The objective of this research is to explore the bulk material properties and failure modes of the coal based carbon foam through experimental and computational analysis. Specifically, mechanical properties and failure modes are assessed through flexure, tensile, and shear tests. In addition, computational models are then developed to further investigate the response and damage mechanisms. This research will provide a better understanding and assessment of material and mechanical properties of carbon foams, thus enabling successful design applications.

2. EXPERIMENTS

2.1 Flexure Experiment

To investigate the failure modes and mechanical properties of the carbon foam core sandwich beams, experiments are conducted according to ASTM Standard C 393, "Flexural Properties of Sandwich Constructions" [22]. Commonly referred to as a four point flexure, this test is used to determine the flexural strength and stiffness of the sandwich by subjecting it to flatwise flexure such that the applied moments produce curvature in the sandwich face sheets. All experiments are conducted using a MTS load frame machine (20 kip load cell with 2 kip range) in the TEES Structures Test Lab at Texas A&M University as seen in Figure 5. The upper fixture remains fixed in place while the lower fixture is moved upward through a pneumatic piston head. The fixtures consist of ½" rollers that evenly distribute the compressive load and minimize crushing as shown in Figure 6.

Figure 5. MTS load frame for flexure experiments

Figure 6. Upper fixture consisting of roller load application for flexure experiments

2.1.1 Specimen Description

Thirty-seven specimens encompassing two distinct core sizes as listed in Table 1 are tested. The density of the carbon foam is nominally 30 lb/ft^3. Each specimen is sized according to guidelines established in ASTM C 393, with the nomenclature shown in Figure 7. L_{total} is the specimen length, b is the specimen width, c is the core thickness, t is the face sheet thickness, and d represents the thickness of one face sheet and the core.

Table 1. Sandwich dimensions

		Core Thickness=0.25 inch	Core Thickness=0.5 inch
L_{total}	Total length [in.]	7.5	13
b	Width [in.]	0.75	1.5
t	Face Sheet Thickness [in.]	0.032	0.032

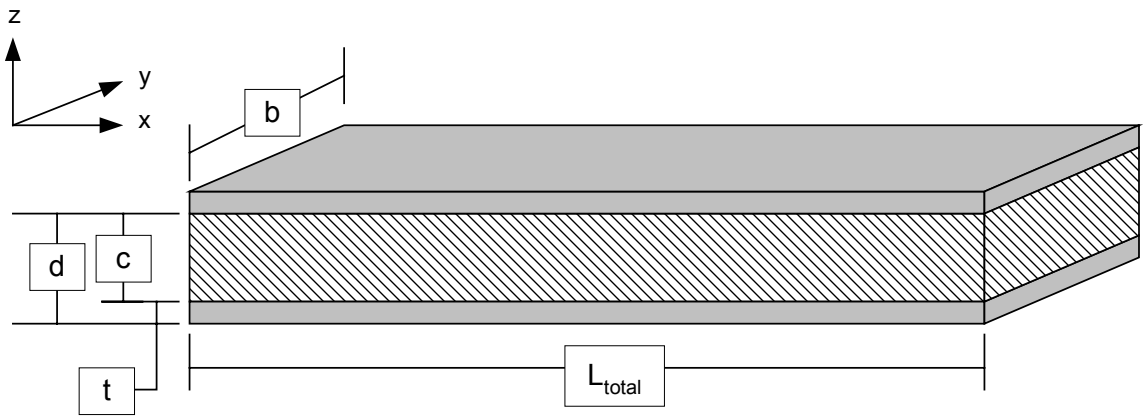

Figure 7. ASTM nomenclature for sandwich specimen

Touchstone Research Laboratories (TRL) assembled the sandwich specimens by adhesively bonding face sheets to their carbon foam core product. The adhesive used to affix the face sheets to the carbon foam cores is West System epoxy with 105 resin and 205-hardener [23]. The majority of the face sheets are provided as a laminate from Kinetic Composites; however, eleven of the specimens are assembled by Adhesive Prepregs for Composite Manufacturers (APCM) using a process of pre-impregnation with epoxy of the carbon fibers or woven mat, known as pre-preg.

The stacking sequence for the Kinetic Composite face sheets from the core out, symmetrically, is one ply of plain weave carbon fiber cloth, 3 plies of carbon fiber uni-tape in a [0/90/0] orientation, and another ply of plain weave carbon fiber cloth as shown in Figure 8.

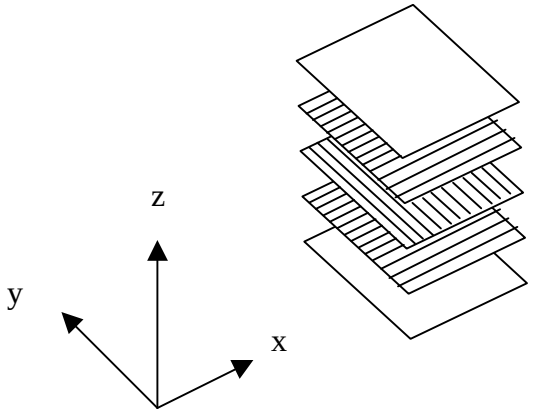

Figure 8. Kinetic Composite face sheet lay-up

Two stacking sequences are used in the face sheets from APCM. Stacking sequence one, shown in Figure 9(a), stacked from the core outward, symmetrically, as plain weave carbon cloth followed by three plies of carbon fiber uni-tape in a [0/90/0] orientation. The second stacking sequence is also symmetric about the core and is presented in Figure 9(b). It consists of carbon fiber uni-tape in a [0/90/0] orientation followed by one ply of plain weave carbon fiber cloth stacked outward from the core.

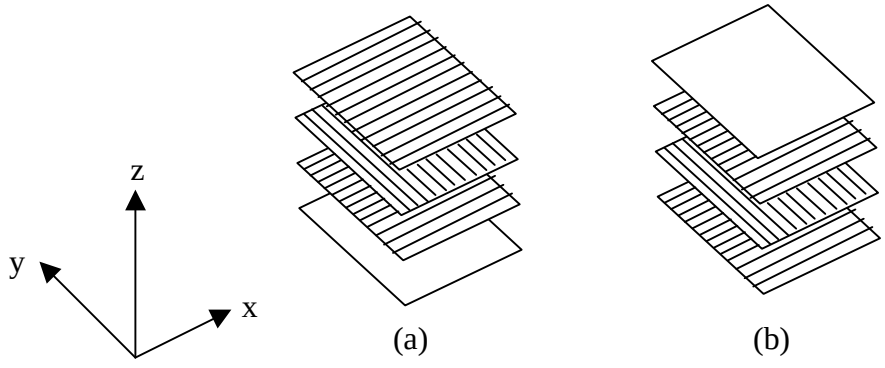

Figure 9. APCM face sheet stacking (a) sequence one (b) sequence two

The face sheet constituent properties are summarized in Table 2. These properties along with stacking sequence are used in classical laminated plate theory (CLPT) to determine apparent properties as listed in Table 3. CLPT is described in detail in section 3.1

Table 2. Material properties for each constituent

	Kinetic Composite Face Sheets		APCM Face Sheets		Carbon Foam
	Plain Weave Carbon Fabric	T300/5280 Uni-Tape	282 Style Carbon Cloth	150 Uni-Tape	
E1 [psi]	1.02E+07	2.63E+07	3.50E+06	1.88E+07	1.50E+05
E2 [psi]	1.02E+07	1.49E+06	3.50E+06	9.40E+06	1.50E+05
G12 [psi]	2.03E+06	1.04E+06	1.17E+06	6.27E+06	4.90E+04
Nu12	0.3	0.28	0.3	0.3	0.35

Table 3. Apparent face sheet properties from CLPT

	Kinetic Composite Face Sheets	APCM Face Sheets
EX [psi]	1.44E+07	9.83E+06
EY [psi]	1.03E+07	8.11E+06
GXY [psi]	1.52E+06	3.66E+06
NuXY	0.176	0.255

The sandwich specimens are divided into sets to account for changes in manufacturing of the carbon foam over the course of the year in which the experiments are conducted. In addition, the sandwich sets are categorized by geometry and face sheet composition according to Table 4.

Table 4. Sandwich set descriptions

	Core Thickness [in]	Face Sheet Lay up
Sandwiches A-E	0.25	Kinetic Composites
Sandwiches F-K	0.5	Kinetic Composites
Sandwiches L-P	0.5	Kinetic Composites
Sandwiches Q-Z	0.5	Kinetic Composites
Sandwiches P1	0.5	APCM 1
Sandwiches P2	0.5	APCM 2

Two specimens are selected for NDE to determine if large voids exceeding the pore size are present in the carbon foam core. The first evaluation is completed using an X-ray technique. These results are difficult to interpret due to the face sheets, which mask the true nature of the core. In some instances, darker areas appear on the X-rays. However, the source of these dark areas is not conclusively traced to voids in the carbon foam. The second evaluation is an ultrasound performed under water. This test did not detect large voids present in the carbon foam core.

2.1.2 Experimental Procedure

A single CEA-series strain gage (uniaxial, gage length of 250 mils, 350 ohm resistance, ±0.5% sensitivity at 24°C) from Micro-measurements is placed in the center of each specimen's face sheet on the compression side and is oriented to record axial strain along the length of the specimen. Each specimen's surface undergoes an extensive cleaning procedure with acetone and alcohol solutions to remove all debris and oil residue prior to mounting the gage in quick set epoxy.

The flexure fixture consists of ½" diameter roller elements that are spaced according to the dimensions listed in Figure 10 as required by ASTM C 393. The standard allows for either a quarter-point loading or a third-point loading scheme and in

this study, quarter-point loading is used. This spacing allows for a balance between the shearing effect and the pure bending.

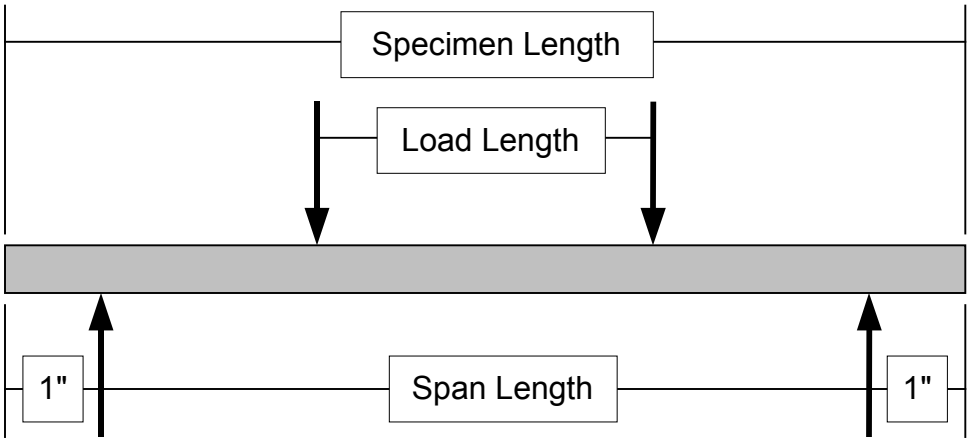

Figure 10. Loading nomenclature for flexure experiments

After mounting the strain gages, the following dimensions are recorded with a dial caliper—specimen length, specimen thickness, specimen width, span and load lengths. The top, right hand side is labeled and the specimen is placed onto the fixture. After centering the specimen, the two load points and two support points are marked on the sandwich cross section for reference purposes to determine the location of damage. The strain gages are attached to the recording device and initialized to ensure accuracy. All experiments are conducted at rates of 0.5 lb/s or 1.0 lb/s, and data is collected using a PC. After failure, the maximum load is recorded and photographs are taken to document the final state of each specimen.

2.1.3 Data Analysis

Initially, data is interpreted from load history graphs for each sandwich. Damage initiation is located by identifying the initial slope change, or point where load carrying capability diminished. All calculations according to ASTM standards are then completed using this damage initiation load and its corresponding strain value.

The initial calculations, as required by ASTM C 393, are undertaken to obtain beam bending stiffness (D) in Equation 1, where E is the face sheet modulus (psi) and b, c, and d as defined in Figure 7.

$$D = \frac{E \cdot (d^3 - c^3) \cdot b}{12} \quad \text{lb-in}^2 \tag{1}$$

Then, the beam shear rigidity (U) is found using Equation 2, where G is the core shear modulus (psi).

$$U = \frac{G \cdot (d + c) \cdot b}{4 \cdot c} \quad \text{lb} \tag{2}$$

The core shear stress and face sheet bending stress are calculated using the damage initiation load (P) and the span length (L) in Equations 3 and 4.

$$\tau = \frac{P}{(d + c) \cdot b} \quad \text{psi} \tag{3}$$

$$\sigma = \frac{P \cdot L}{4 \cdot t \cdot (d + c) \cdot b} \quad \text{psi} \tag{4}$$

Finally, the sandwich beam deflection (Δ) due to both bending and shear is calculated using Equation 5.

$$\Delta = \frac{11 \cdot P \cdot L^3}{768 \cdot D} + \frac{P \cdot L}{8 \cdot U} \quad \text{in} \tag{5}$$

2.1.4 Experimental Flexure Results

The load history of a typical sandwich specimen is shown in Figure 11, where the load is negative due to the sign convention associated with compressive loading. This is the curve used to determine the first slope change and damage initiation in each sandwich. Notice that the curve is smooth for this specimen indicating that the sandwich was able to hold and redistribute the load well. When the curve begins to step and show plateaus, this indicates that the sandwich is not able to redistribute the load as well; thus this is the area studied for slope changes indicating damage initiation. In Figure 11, the slope change is highlighted with the bold lines indicating slope, and the damage initiation point is marked with an arrow. In addition, Figure 12 shows the strain history plot for the same sandwich specimen.

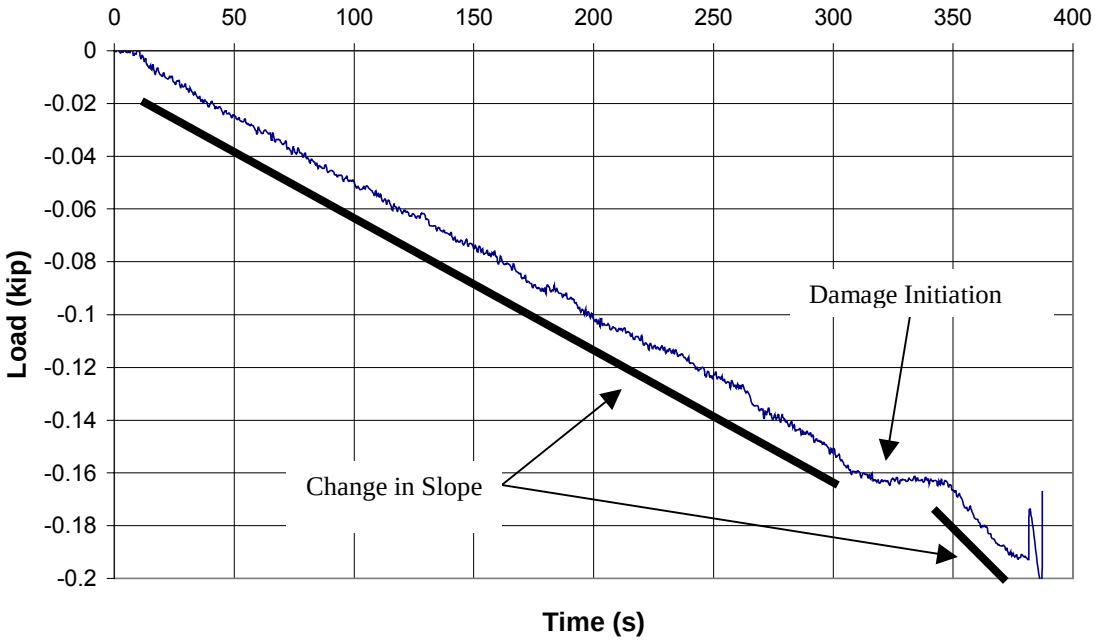

Figure 11. Typical load history plot from flexure experiments

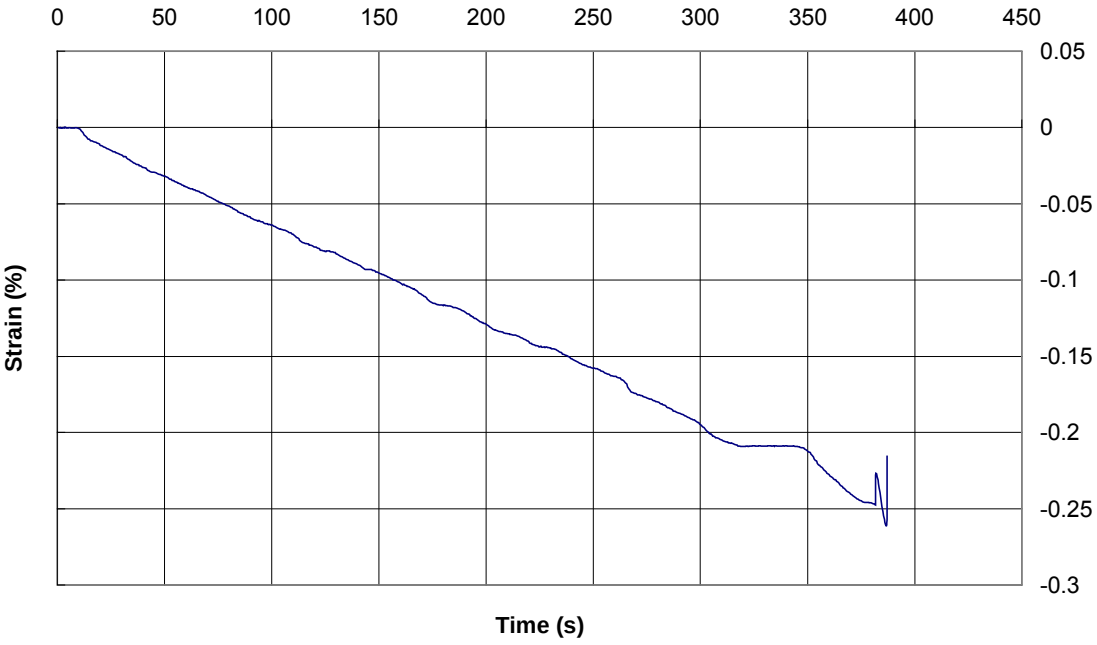

Figure 12. Typical strain history plot from flexure experiments

The load versus strain plots for each of the specimens is linear in nature as in Figure 13, without the change in slope. The absence of a slope change may be a reflection of the resolution of the graph and measurement devices; however, the linear nature indicates that material nonlinearity is not a concern for the carbon foam. Note that the strain is negative because it is measured on the compressive face sheet; the load is negative as well due to compressive load sign convention.

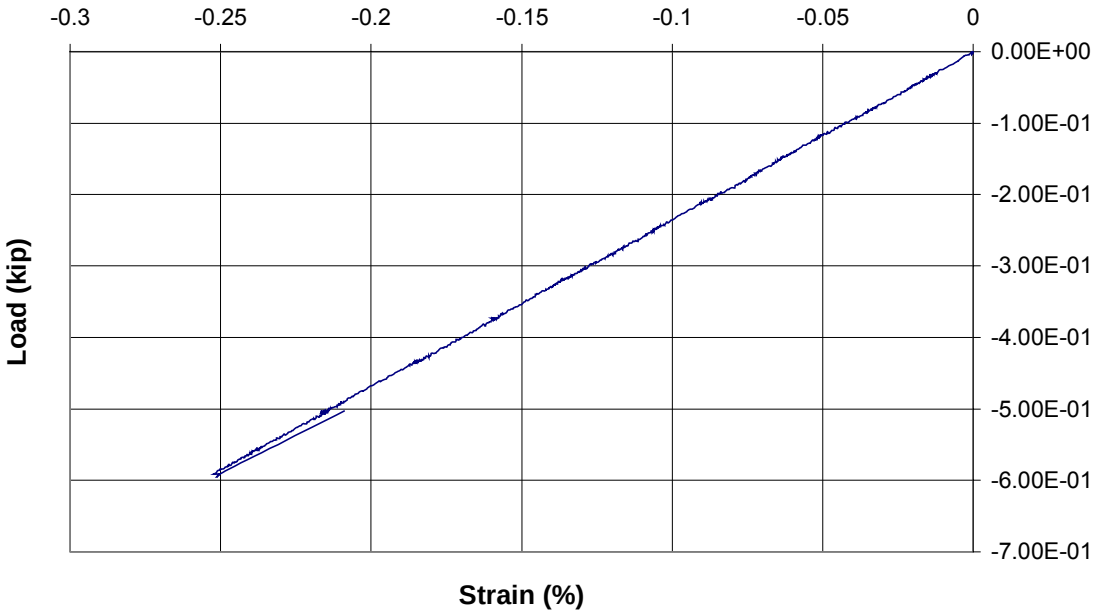

Figure 13. Typical load versus strain plot from flexure experiments

In each specimen, damage initiates at either the left, or the right loading point due to a complex stress state at the load point. Shear cracks then develop in the region between the load point and support point. Finally, the foam begins fracturing into smaller pieces until total failure is reached. Although delamination does occur in some areas, the majority of the specimen face sheets remain rough in texture indicating that the main mode of failure is not delamination driven. A crack indicating damage

initiation is shown in Figure 14, while Figure 15 depicts a typical final failure seen in the experiment.

Figure 14. Damage initiation crack in sandwich specimens

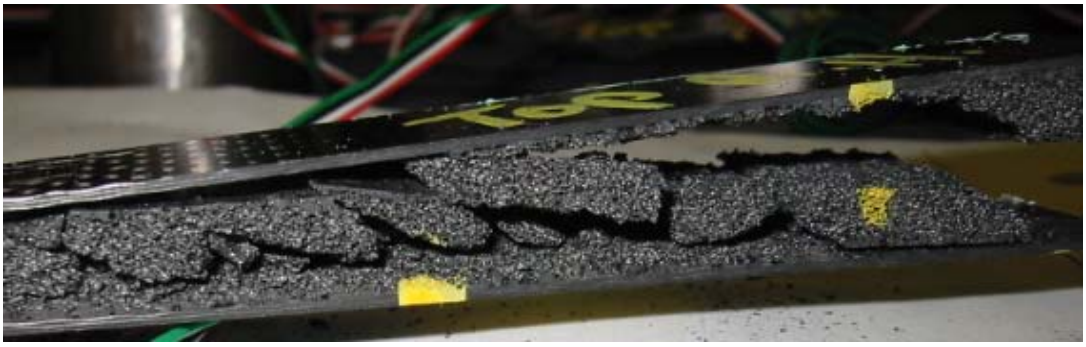

Figure 15. Typical final failure of sandwich specimens

The average load at damage initiation, along with the strain at that load, varies across the various batches of sandwich specimens tested as well as within the sets of sandwiches. Thirty-seven specimens are tested over the span of a year, during which changes in the carbon foam manufacturing occurred. Therefore, the results presented are separated into sets, to account for any variation due to the manufacturing of the foam, as well as changes in geometry and face sheet composition. The variation within the individual sandwich sets for axial strain measured at damage initiation is presented in Figure 16. Note that the load history plots obtained for sandwiches L-P are not as

smooth as for other sets, and determining the first slope change is more difficult. A summary of the average load and strain values measured for each set of specimens at damage initiation and final failure is presented in Table 5. While the load carried shows dependency on the core thickness, the strain at damage initiation is independent of face sheet lay-up and core thickness.

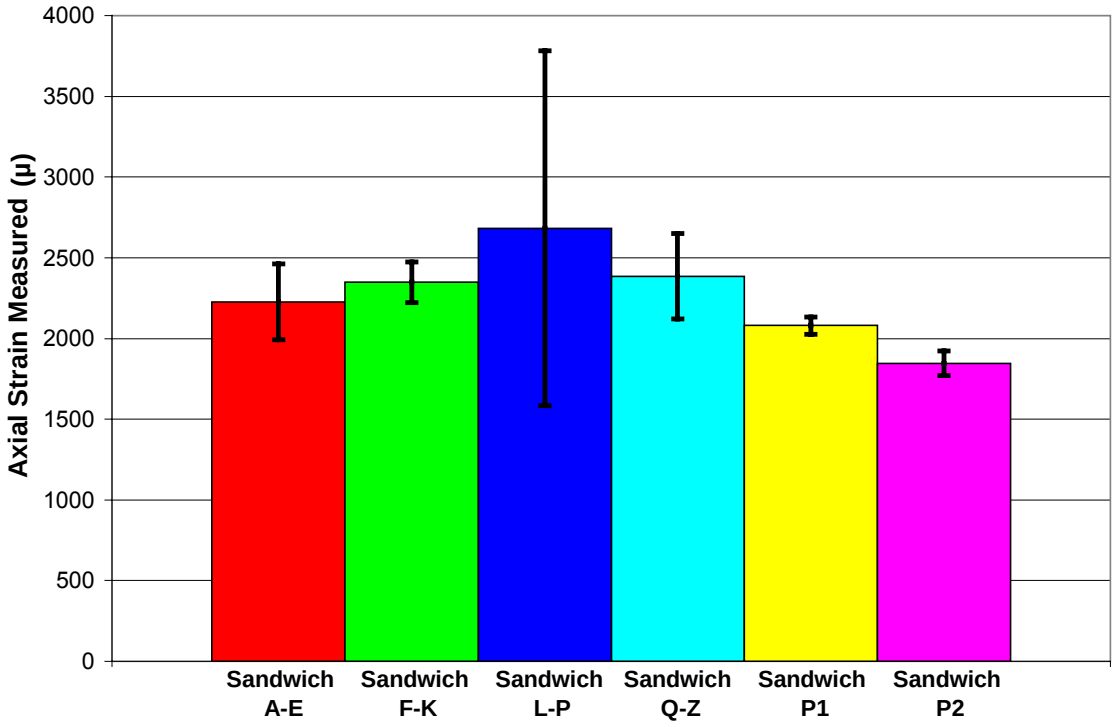

Figure 16. Axial strain at damage initiation during flexure experiments

Table 5. Summary of strain values recorded during flexure experiments

	Damage Initiation		Final Failure	
	Load [lbs]	Strain [μ]	Load [lbs]	Strain [μ]
Sandwiches A-E	165	2226	202	2705
Sandwiches F-K	543	2349	600	2622
Sandwiches L-P	395	2684	490	3373
Sandwiches Q-Z	251	2386	277	2650
Sandwiches P1	399	2080	415	2153
Sandwiches P2	352	1845	377	2004
Average	--	2262	394	2585
Standard Deviation	--	286	143	483

The ASTM calculation results are presented in Table 6. The values presented are averages for each set of specimens along with the standard deviation for each set. The sandwich core shear stress and central (or maximum) deflection calculations are compared to computational predictions in sections 3.2-3.4.

Table 6. ASTM C 393 flexure parameters

Specimens	Panel Bending Stiffness	Panel Shear Rigidity	Core Shear Stress	Face Bending Stress	Sandwich Panel Deflection
	D [lb-in^2]	U [lb]	τ [psi]	σ [psi]	Δ [in]
Sandwich A-E	6340	10870	397	16918	0.071
Standard Deviation A-E	67	85	39	1721	0.008
Sandwich F-K	47588	39987	343	29581	0.238
Standard Deviation F-K	1010	721	20	1799	0.016
Sandwich L-P	48120	40235	248	21386	0.171
Standard Deviation L-P	196	141	46	3929	0.032
Sandwich Q-Z	47833	40160	158	13584	0.109
Standard Deviation Q-Z	484	345	15	1315	0.011
Sandwich P1	32464	39983	252	21730	0.250
Standard Deviation P1	305	316	2	185	0.003
Sandwich P2	32432	39938	223	19198	0.221
Standard Deviation P2	477	562	19	1643	0.019

2.2 Tensile Experiment

Additional tensile experiments are performed on the carbon foam alone according to ASTM Standard C 297 "Flatwise Tensile Strength of Sandwich Constructions" [24]. Although the standard can be used to test full sandwich panels, it is also used on the core material alone without the face sheets. This experiment consists of subjecting the sandwich core material to tension to determine the tensile strength and modulus of the carbon foam core. This series of experiments is performed using a MTS load frame machine (20 kip load cell with 2 kip range) in the TEES Structures Test Lab at Texas A&M University.

2.2.1 Specimen Description

The twelve specimens listed in Table 7 are prepared and tested according to ASTM C 297. The carbon foam has a nominal density of 17 lb/ft^3, which is not the same density as the carbon foam utilized in the sandwich beams. Thus no comparison can be made relating the two tests. Specifications for a straight-edged specimen, i.e. without dog-bond configuration, are presented in Figure 17. L_{total} is the total specimen length, L_{gage} is the ungripped, or untabbed section, b is the specimen width and t is the specimen thickness.

Table 7. Specimen dimensions for tensile experiments

Symbol	Description	Value
L_{total}	Total Length [in.]	7
L_{gage}	Gage Length [in.]	3
b	Width [in.]	1
t	Thickness [in.]	0.5

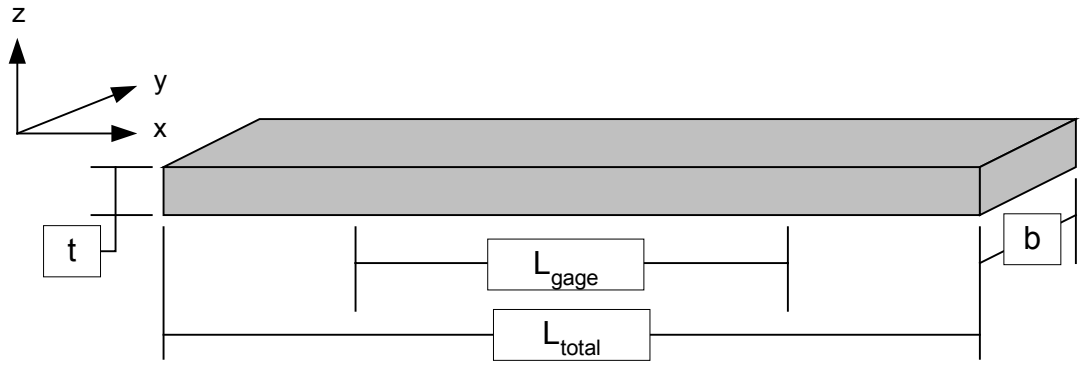

Figure 17. ASTM nomenclature for tension specimens

Six of the specimens are tested by gripping the carbon foam specimen directly as seen in Figure 18. The other six are tested in a pin fixture as seen in Figure 19. Fiberglass tabs are bonded to the carbon foam using room cure epoxy, and then the specimens are loaded through a steel pin inserted through the two tabs on either end of the specimen as in Figure 20.

Figure 18. Direct grip fixture for tension experiments

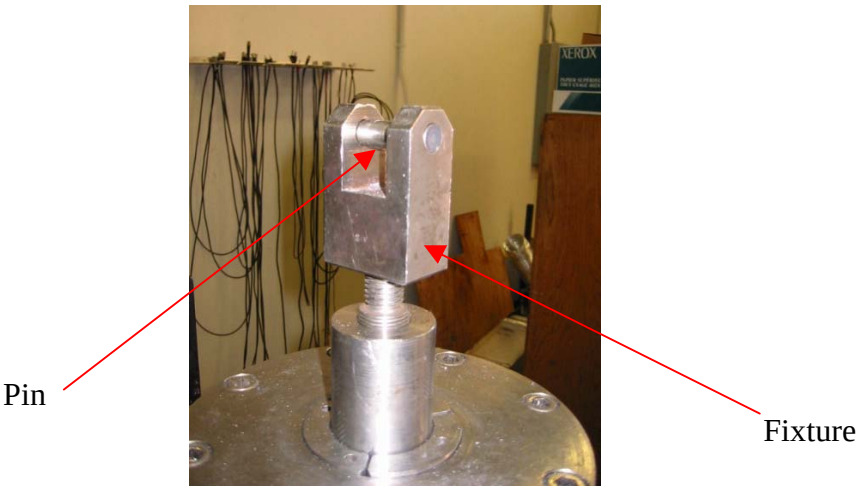

Figure 19. Pin tabbed fixture for tension experiments

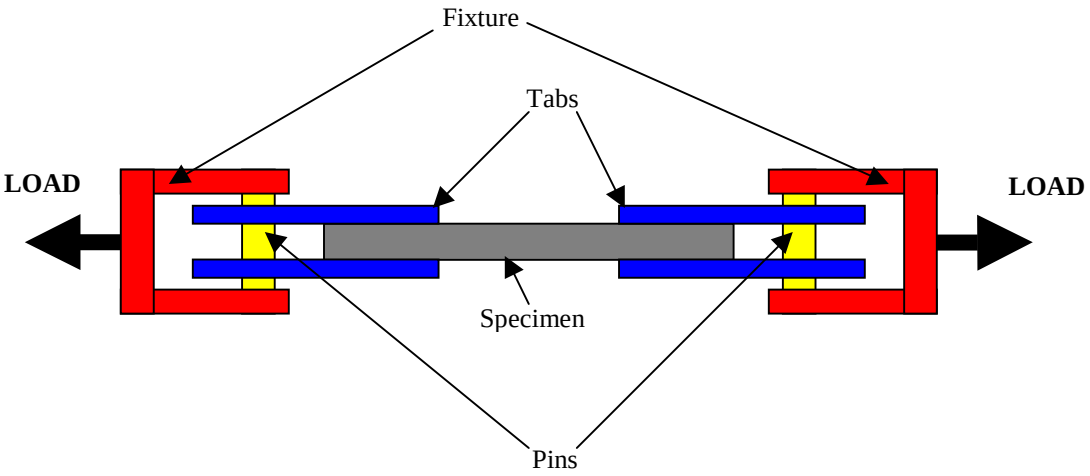

Figure 20. Load application in pin tabbed fixture

2.2.2 Experimental Procedure

The total specimen length, width and thickness are measured with a dial caliper before loading the specimen into the desired fixture. When the direct grip fixture is used, care is taken to prevent crushing of the foam through over tightening. This is achieved by closing the fixture jaws until they come in contact with the specimen surface. Then the tightening screw is turned two additional revolutions. For the pin tab fixture, as much slack as possible is removed, while minimizing pre-load.

After mounting the specimen into the fixture, the gage length is measured with calipers. The specimens directly gripped by the fixture are tested at rates ranging from 0.1 in./minute to 0.25 in./minute. The pin tabbed specimens are tested at rates ranging from 0.005 in./minutes to 0.05 in./minute. Both the load and the corresponding crosshead displacement are recorded. After failure, the maximum load and failure location are identified, and digital photographs are taken to document the final state of each specimen.

2.2.3 Data Analysis

Initially, original data consist of crosshead displacement and load applied. The crosshead displacement (*chd*) along with the initial gage length (L_{gage}) are used to obtain strain (ε) in Equation 6.

$$\varepsilon = \frac{\Delta Length}{OriginalLength} = \frac{chd}{L_{gage}} \quad \text{in./in.} \tag{6}$$

Stress (σ) is estimated according to Equation 7, where *P* is the load applied and *A* is the cross sectional area of the specimen defined in Figure 16.

$$\sigma = \frac{P}{A} = \frac{P}{bt} \quad \text{psi} \tag{7}$$

The stress is then plotted as a function of strain. From these graphs, the Young's modulus is found as the slope of the initial linear section.

2.2.4 Experimental Tensile Results

The specimens gripped directly tend to fracture straight across the width of the specimen as seen in Figure 21. However, every specimen fails inside the gripped area and not in the gage length, thus preventing any conclusive evidence of tensile strength. In most cases, audible slipping sounds are noted as the experiments are conducted.

Figure 21. Typical final failure of directly gripped tension specimens

The average modulus obtained in the directly gripped specimens is 31.51 psi, with a standard deviation of 34.73, indicating that this method is not acceptable for obtaining the Young's modulus of carbon foam.

Due to the poor results obtained with the directly gripped fixture, more tests were performed using the pin tabbed fixture. A typical stress strain plot obtained for a pin tabbed specimen appears in Figure 22. While some specimens exhibit a single Young's modulus (the boxed value), others exhibit multiple distinct moduli over the stress-strain ranges. However, typically one modulus dominated the range of the data, thus the initial portion was neglected as a settling period in cases where multiple moduli were observed.

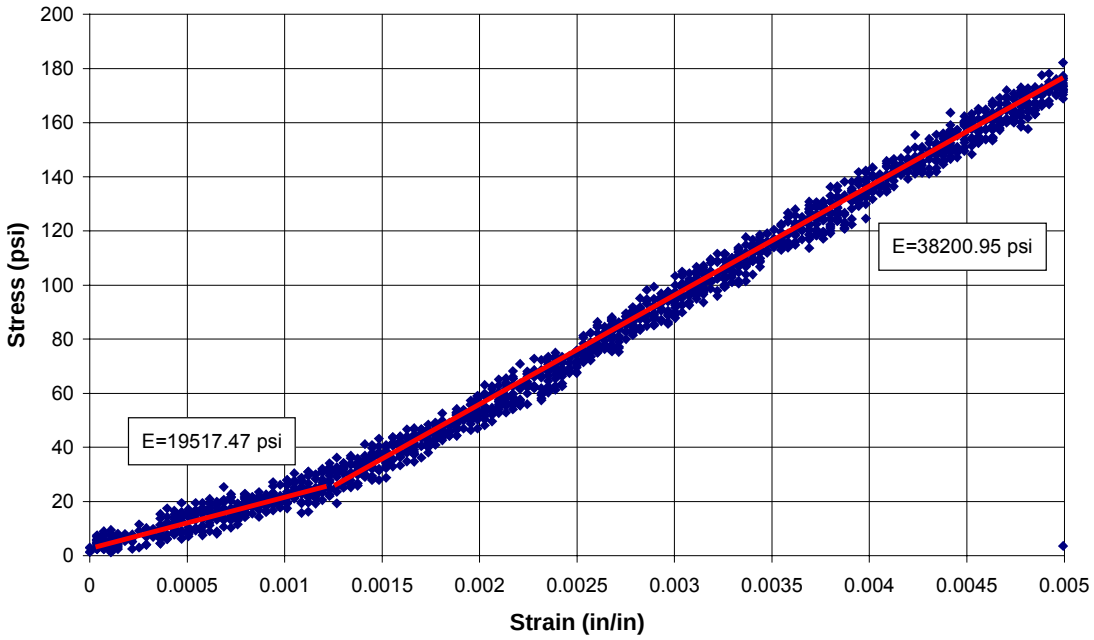

Figure 22. Example stress-strain plot obtained for a pin tabbed specimen

The pin tabbed specimens tend to fracture straight across the specimen width as well. In all cases, the fracture surface is in close proximity to the tab connection point preventing any conclusive evidence with regard to tensile strength. An example of a pin tab specimen fracture is shown in Figure 23. The results for the pin-tabbed specimens indicate an average Young's modulus of 39 ksi, with a standard deviation of 8.25 ksi. The manufacturer reports a value for Young's modulus as 30 ksi [1].

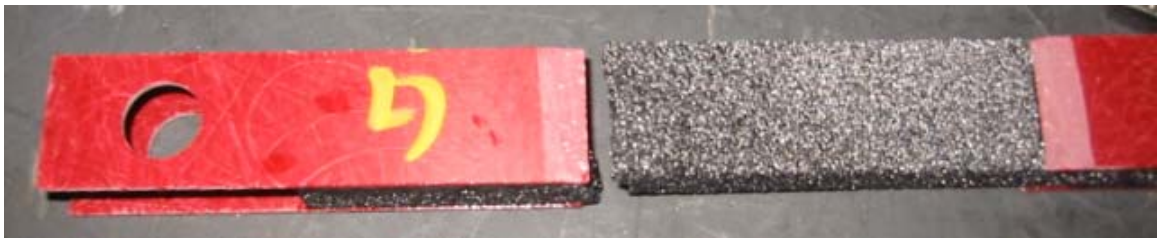

Figure 23. Typical final failure of pin tabbed tension specimens

2.3 Iosipescu Experiment

The carbon foam is also subjected to shear loads according to ASTM Standard C 1292 “Shear Strength of Continuous Fiber-Reinforced Advanced Ceramics at Ambient Temperatures” [25]. This experiment covers the determination of shear strength and modulus according to two methods—the double notched specimen and the Iosipescu experiment. For this research, the Iosipescu experiment is chosen.

The experiments are performed at the TEES Structures Test Lab at Texas A&M University using a standard Iosipescu fixture, seen in Figure 24, mounted in the MTS load frame (100 lb. load cell). This fixture consists of a stationary element mounted on a base plate, and a movable element capable of vertical translation guided by a stiff post. This arrangement produces four point asymmetric flexure that tends to shear the specimen as seen in Figure 25. A notch ensures that the initiation is at the midpoint of the specimen.

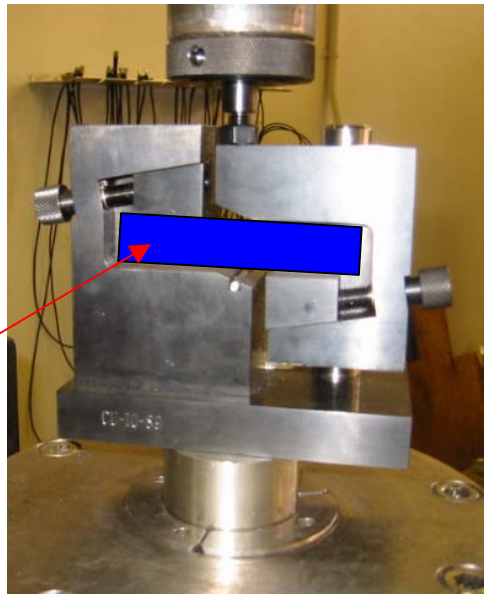

Figure 24. Fixture used for Iosipescu experiments

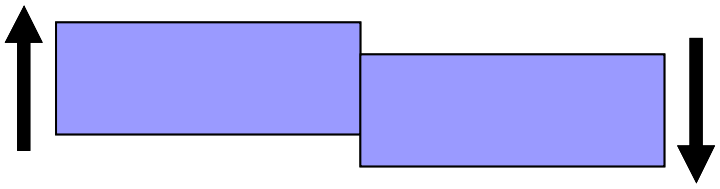

Figure 25. Shearing effect created with the Iosipescu fixture

2.3.1 Specimen Description

Six specimens, with a nominal density of 17 lb/ft^3, which is different from the sandwich carbon foam density, are sized and tested according to ASTM C 1292 with the specimen geometry as described in Figure 26. L is the specimen length, w is the specimen width, t is the specimen thickness, θ is the notch angle, r is the radius of the notch corner and h is the distance between notches. The specimen specifications are listed in Table 8.

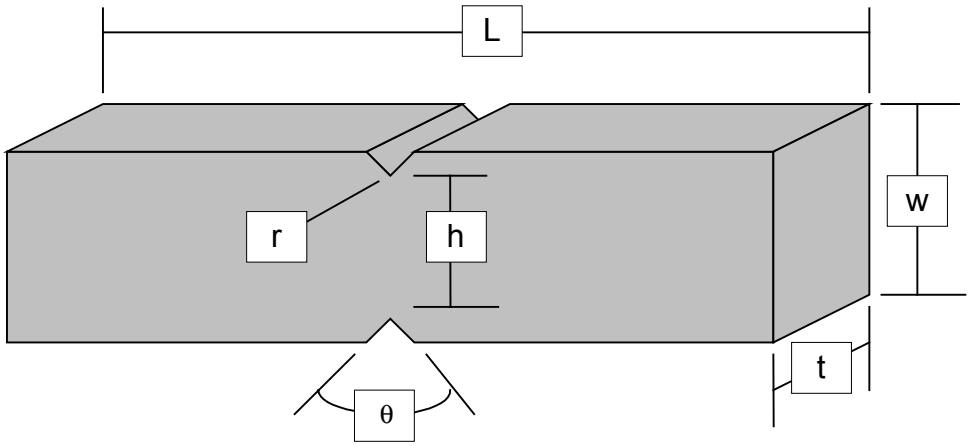

Figure 26. ASTM nomenclature for Iosipescu experiments

Table 8. Specimen dimensions for Iosipescu experiments

Symbol	Description	Value
L	Length [in.]	2.9
w	Width [in.]	0.75
t	Thickness [in.]	0.5
θ	Notch Angle [degrees]	90
r	Notch Radius [in.]	0.05
h	Distance between Notches [in.]	0.4

2.3.2 Experimental Procedure

Initially, each specimen is measured with dial calipers for the thickness and width of the gage section. The experiment fixture is positioned so that the two grips aligned vertically. The specimen is then placed loosely into both grips and pushed back so it touches the back wall of the fixture. The alignment tool is used to ensure the proper position of the notch at the midpoint of the specimen. The lower grip is then tightened, and the upper grip position adjusted until it just touches the specimen without pre-loading it. The upper grip is then tightened into place.

The experiment is conducted at a rate of 0.025 mm per second (0.059 in per minute) controlled by a computer that records the crosshead displacement and the load applied. After failure, the dimensions of the failed shear area are taken with dial calipers. In addition, photographs are taken to document the final state of each specimen.

2.3.3 Data Analysis

The original data is manipulated to obtain the shear strain and shear stress to estimate the shear modulus. The shear strain (γ) can be interpreted according to Equation 8 where the quantities α, δ and L are as depicted in Figure 27. Note that the

specimen does not actually rotate during the experiment; rather the two halves of the specimen move vertically relative to each other as in Figure 25.

$$\gamma = \tan(\alpha) = \frac{2\delta}{L} \qquad \text{in/in} \tag{8}$$

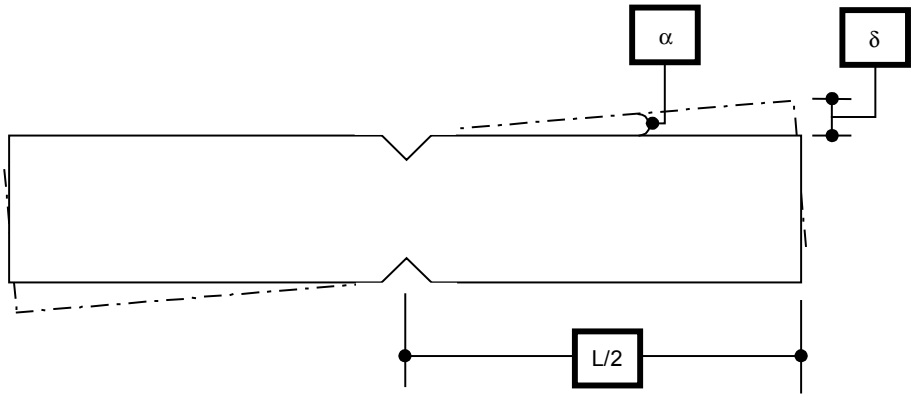

Figure 27. Nomenclature for shear strain calculation

The stress (σ) is obtained with Equation 9 where *P* is the applied load, and *A* is the gage section area, where *t* is the specimen thickness and *h* is the distance between notches as seen in Figure 26.

$$\sigma = \frac{P}{A} = \frac{P}{ht} \qquad \text{lb-in}^2 \tag{9}$$

The shear stress is then plotted against the shear strain. From these graphs, the shear modulus is found as the slope of the linear portion.

2.3.4 Experimental Iosipescu Results

A typical stress strain plot obtained in the Iosipescu experiment appears in Figure 28. The average applied final load for all specimens is 33 lbs with a standard deviation of 5 lbs. The average shear modulus is 21 ksi with a standard deviation of 8 ksi.

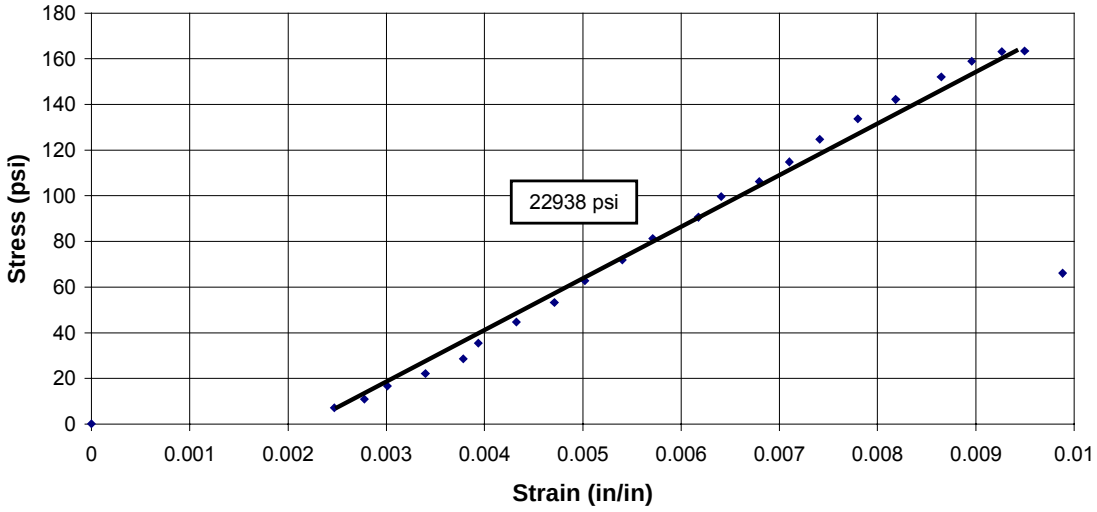

Figure 28. Example stress-strain plot obtained for an Iosipescu specimen

All specimens fail when a shear crack at approximately 45° formed as expected. Approximately one-half exhibit a single shear crack, while the remaining specimens have double shear cracks. The failure mode for a majority of the specimens also points towards the top V notch as the origin of the shear cracking. Typical specimen failures are shown in Figure 29.

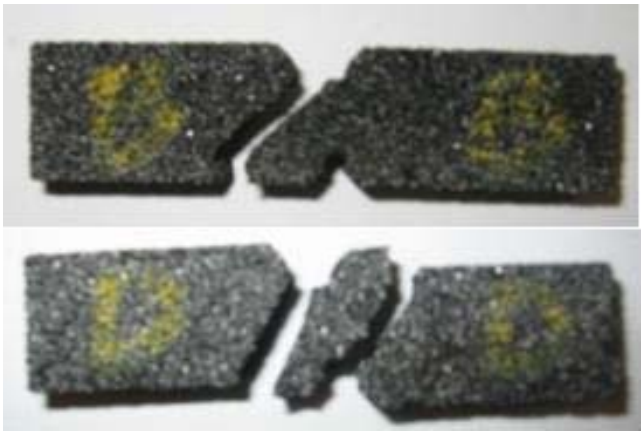

Figure 29. Typical final failure of Iosipescu experiments

3. COMPUTATIONAL ANALYSIS

3.1 Classical Laminated Plate Theory

The initial computational analysis conducted is based on classical laminated plate theory (CLPT) where the orthotropic nature of the individual ply or lamina [26] is taken into account when evaluating the overall laminate stiffness, as well as the ply level stresses and strains. This approach provides a basic model to investigate the strains and displacements of the carbon foam core sandwich beam under flexure loads. The sandwich beam is represented by the individual plies of the face sheets and the carbon foam core. The ply level orthotropic Hooke's law, as expressed in Equation 10, refers to the material coordinates, where 1 is in the direction of the fiber, and 2 is transverse to the fiber. [Q] is the stiffness matrix and depends on the material properties E_1, E_2, G_{12} and υ_{12}. This ply level relationship is then transformed into a global coordinate system that is consistent with the loading as shown in Equation 11 and 12, where [T_σ] and [T_ε] are transformation matrices of directional cosines.

$$\begin{bmatrix} \sigma_1 \\ \sigma_2 \\ \tau_6 \end{bmatrix}_k = \begin{bmatrix} Q_{11} & Q_{12} & 0 \\ Q_{12} & Q_{22} & 0 \\ 0 & 0 & Q_{66} \end{bmatrix}_k \begin{bmatrix} \varepsilon_1 \\ \varepsilon_2 \\ \gamma_6 \end{bmatrix}_k \tag{10}$$

$$\begin{bmatrix} Q_{xx} & Q_{xy} & Q_{xs} \\ Q_{yx} & Q_{yy} & Q_{ys} \\ Q_{sx} & Q_{sy} & Q_{ss} \end{bmatrix}_k = [T_\sigma]_k \begin{bmatrix} Q_{11} & Q_{12} & 0 \\ Q_{12} & Q_{22} & 0 \\ 0 & 0 & Q_{66} \end{bmatrix}_k [T_\varepsilon]_k \tag{11}$$

$$\begin{bmatrix} \sigma_x \\ \sigma_y \\ \tau_{xy} \end{bmatrix}_k = \begin{bmatrix} Q_{xx} & Q_{xy} & Q_{xs} \\ Q_{xy} & Q_{yy} & Q_{ys} \\ Q_{sx} & Q_{sy} & Q_{ss} \end{bmatrix}_k \begin{bmatrix} \varepsilon_x \\ \varepsilon_y \\ \gamma_s \end{bmatrix}_k \tag{12}$$

In addition, the strain vector is expanded by the nominal strain on the reference surface and the contribution from the laminate curvature in the through-the-thickness direction as given in Equation 13. The global stress-strain relationship for an individual ply is then obtained in Equation 14 by substituting this strain expansion relationship into Equation 12.

$$\begin{bmatrix} \varepsilon_x \\ \varepsilon_y \\ \gamma_s \end{bmatrix} = \begin{bmatrix} \varepsilon_x^o \\ \varepsilon_y^o \\ \gamma_s^o \end{bmatrix} + z \begin{bmatrix} \kappa_x \\ \kappa_y \\ \kappa_s \end{bmatrix} \tag{13}$$

$$\begin{bmatrix} \sigma_x \\ \sigma_y \\ \tau_{xy} \end{bmatrix}_k = \begin{bmatrix} Q_{xx} & Q_{xy} & Q_{xs} \\ Q_{xy} & Q_{yy} & Q_{ys} \\ Q_{sx} & Q_{sy} & Q_{ss} \end{bmatrix}_k \begin{bmatrix} \varepsilon_x^o \\ \varepsilon_y^o \\ \gamma_s^o \end{bmatrix}_k + z \begin{bmatrix} Q_{xx} & Q_{xy} & Q_{xs} \\ Q_{xy} & Q_{yy} & Q_{ys} \\ Q_{sx} & Q_{sy} & Q_{ss} \end{bmatrix}_k \begin{bmatrix} \kappa_x \\ \kappa_y \\ \kappa_s \end{bmatrix}_k \tag{14}$$

Finally, the equations of equilibrium (or force/moment resultant equations) are obtained by summation of forces and moments to obtain resultants in the global coordinates for the laminate as shown in Equation 15. In the ABD matrix, *A* represents the extensional stiffness of the laminate, *D* describes the bending stiffness and *B* is the

bending/extensional coupling stiffness. The exact equations to calculate the ABD matrix terms are shown in Equations 16-18.

$$\begin{bmatrix} N_x \\ N_y \\ N_s \\ -- \\ M_x \\ M_y \\ M_s \end{bmatrix} = \left[\begin{array}{ccc|ccc} A_{xx} & A_{xy} & A_{xs} & B_{xx} & B_{xy} & B_{xs} \\ A_{yx} & A_{yy} & A_{ys} & B_{yx} & B_{yy} & B_{ys} \\ A_{sx} & A_{sy} & A_{ss} & B_{sx} & B_{sy} & B_{ss} \\ - & - & - & - & - & - \\ B_{xx} & B_{xy} & B_{xs} & D_{xx} & D_{xy} & D_{xs} \\ B_{yx} & B_{yy} & B_{ys} & D_{yx} & D_{yy} & D_{ys} \\ B_{sx} & B_{sy} & B_{ss} & D_{sx} & D_{sy} & D_{ss} \end{array}\right] \begin{bmatrix} \varepsilon_x^o \\ \varepsilon_y^o \\ \varepsilon_s^o \\ -- \\ \kappa_x \\ \kappa_y \\ \kappa_s \end{bmatrix} \tag{15}$$

$$A_{ij} = \sum_{k=1}^{n} Q_{ij}^k (h_k - h_{k-1}) \tag{16}$$

$$B_{ij} = \frac{1}{2} \sum_{k=1}^{n} Q_{ij}^k (h_k^2 - h_{k-1}^2) \tag{17}$$

$$D_{ij} = \frac{1}{3} \sum_{k=1}^{n} Q_{ij}^k (h_k^3 - h_{k-1}^3) \tag{18}$$

The inherent CLPT assumptions are (i) thickness dimension of the laminate is much smaller than the lateral, or beam, dimensions of the laminate, (ii) all displacements are much smaller than the thickness of the laminate and (iii) Kirchhoff's hypothesis

holds, i.e. normal lines remain normal to the neutral surface, and in-plane displacements vary linearly through the thickness of the laminate.

For the special case of a balanced, symmetric laminate, as in the case of the sandwich beam, the apparent laminate properties are evaluated as in Equation 19-23, where h is the total laminate thickness. A balanced laminate is one in which pairs of plies with identical thickness and elastic properties exist but have +θ and –θ orientations of the principal material axis with respect to the global coordinates.

$$\overline{E_x} = \frac{1}{h}\left[A_{xx} - \frac{A_{xy}^{\,2}}{A_{yy}} \right] \tag{19}$$

$$\overline{E_y} = \frac{1}{h}\left[A_{yy} - \frac{A_{xy}^{\,2}}{A_{xx}} \right] \tag{20}$$

$$\overline{\upsilon_{xy}} = \frac{A_{xy}}{A_{yy}} \tag{21}$$

$$\overline{\upsilon_{yx}} = \frac{A_{xy}}{A_{xx}} \tag{22}$$

$$\overline{G_{xy}} = \frac{A_{ss}}{h} \tag{23}$$

A convenient computer software package based on CLPT formulation, The Laminator, is used to obtain the overall stiffness, and ply level stresses and strains for the carbon foam core sandwich beam [27]. An example of the stacking sequence input appears in Table 9. Material properties provided by the manufacturer, for the individual constituents are listed in Table 2 in section 2.1. Although the face sheet constituents are orthotropic, the carbon foam core is considered to be isotropic on a macroscopic scale.

Table 9. CLPT stacking sequence input

Layer	Material	Ply Angle	Ply Thickness [mils]
1	Plain Weave Cloth	0	8.5
2	Uni-tape	0	6
3	Uni-tape	90	6
4	Uni-tape	0	6
5	Plain Weave Cloth	0	8.5
6	Carbon Foam	0	0.125
7	Carbon Foam	0	0.125
8	Plain Weave Cloth	0	8.5
9	Uni-tape	0	6
10	Uni-tape	90	6
11	Uni-tape	0	6
12	Plain Weave Cloth	0	8.5

The mechanical load applied to the sandwich beam is the average moment at damage initiation as observed from the experimental four point flexure data for each set of sandwiches. This mechanical load is depicted in Figure 30, where P is the average load at damage initiation. After applying the mechanical load for each set of sandwiches, the corresponding axial strain on the top surface of ply 1 is recorded for comparison to the axial strain data recorded in the experiment.

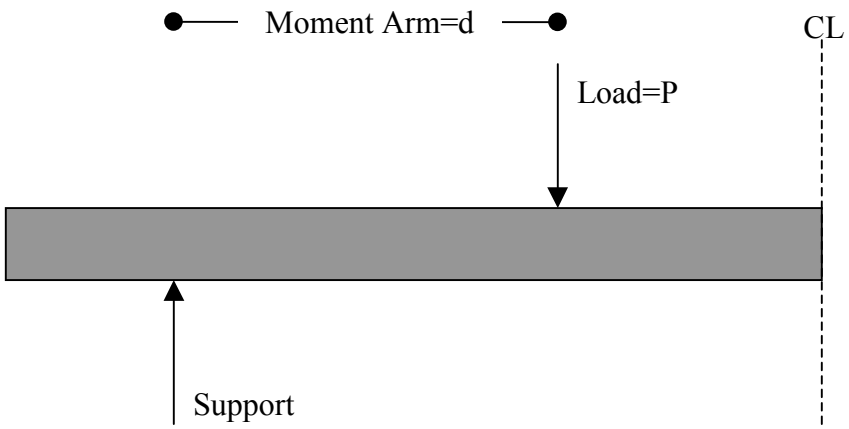

Figure 30. Moment (P*d) applied in Laminator

The results obtained from The Laminator are tabulated in Table 10, where the mechanical load is equivalent to average moment at damage initiation during experiments. M_x represents the applied load in The Laminator and ε_x represents the predicted strain.

Table 10. Comparison of CLPT results for average moment at damage initiation

	Moment Ratio Mx/Mexperiment	Strain Ratio Єx/Єexperiment
Specimen A-E	1	0.37
Specimen F-K	1	1.19
Specimen L-P	1	0.76
Specimen Q-Z	1	0.54
Specimen P1	1	1.55
Specimen P2	1	1.51

The strain of interest is the axial strain on the top surface of the uppermost ply where the strain gage is mounted during experimental flexure testing. For comparison purposes, when the strain ratio of analytical to average experimental value is unity, the results are considered to be in complete agreement with the average measured strain during flexure experiments. There appears to be consistency in the value predicted for the two sets of APCM face sheet specimens (P1 and P2); however, no consistency appears amongst the 0.5" core sets (F-K, L-P and Q-Z). In some cases, analytical predictions match the average strain gage data, but mostly they are likely to over or under estimate it. This indicates that this method is not appropriate for predicting strains, or damage initiation in the carbon foam sandwich beams. The likely source of difference in this analysis is violation of the assumptions used. For example, the sandwich thickness is generally not much smaller than the beam dimensions—thickness of 0.5" compared with the beam dimensions of 1.5" x 13". Also, the vertical displacements are too large in comparisons to the sandwich thickness to be considered small displacements—displacements of 0.2" compared to a thickness dimension of 0.5".

The apparent laminate properties of the various face sheet lay-ups in the sandwich beams are presented in Table 3 in section 2 as obtained from Equations 19-23.

These values are used in the ASTM C 393 data reduction calculations for the flexure experiments, as well as the finite element models of the flexure study described in section 3.2-3.4.

3.2 Finite Element Flexural Study

The four point flexure experiment conditions are simulated with a commercial FEA program, Cosmos M [28]. The sandwich construction is represented with a single, homogenized face sheet layer, carbon foam core and another homogenized face sheet layer. Since face sheet failure is not observed in the experiments, single layer representation reduces the total number of elements required, without sacrificing accuracy. Both linear displacements and linear elastic constitutive behavior are assumed in the initial model. The mesh consists of 8-node brick elements, with 6 degrees of freedom. In the 0.25" core sandwiches, 528 elements are used in each homogenized face sheet and the core is composed of 1,584 elements. Through the thickness, the face sheets are one element thick and the core is 3 elements thick. For the 0.5" core, 960 elements are used in each face sheet and 4,800 element compose the core. The face sheets are one element thick, while the core is 5 elements thick. These numbers represent approximately equal number of elements per unit length between the two core size sandwiches. No convergence study was undertaken to determine the effect of the number of elements in the model.

3.2.1 Material Properties

The apparent laminate properties of the face sheet lay-up obtained with CLPT are used along with manufacturer supplied properties of the carbon foam core as presented in Table 3 in section 2.1. The face sheets are orthotropic in nature, while the carbon

foam is considered isotropic. Although the porous nature of the carbon foam can introduce anisotropy to the problem from non-uniform density gradients, on a macroscopic scale isotropy is an acceptable assumption.

3.2.2 Boundary Conditions and Loading

The model is restrained and loaded to simulate the four point flexure experiment. Displacement boundary conditions are placed on all nodes along two parallel lines on the bottom surface of the bottom face sheet to prevent translation in two directions, *Y* and *Z*, as seen in Figure 31. In addition, a single node on one side is restrained from translation in the *X* direction. This method of applying the restraints allows axial slip during loading, which mimics the effect of applying the force through rollers in the flexure experiment. Dimensions *L* and *b* refer to the specific dimensions of the sandwich panel as described in Table 1 in section 2.1, and *h* represents to overall height of the sandwich beam (two face sheets + carbon foam core).

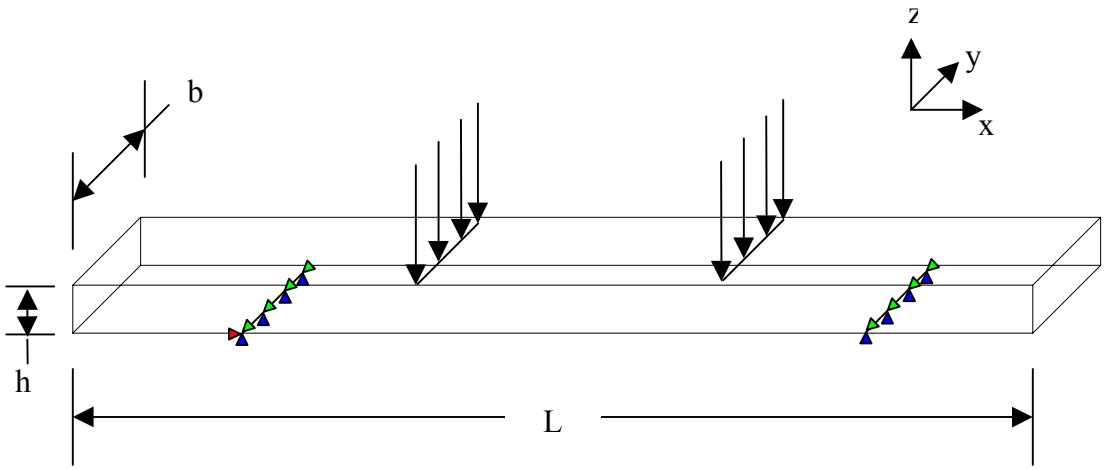

Figure 31. Schematic of FEA boundary conditions and loading

Uniform load per unit length is also applied along two parallel lines on the top surface of the sandwich beam. Each node on the lines carries an equal distribution of the total load, as shown in Figure 31. The total load is determined from experimental data as the average load at damage initiation for each set of sandwiches, and is completely applied in a single analysis step.

3.2.3 Finite Element Analysis Results

Several plots are generated for each set of sandwich specimens. Examples of the deformation, displacement, shear stress and axial strain plots appear in Figure 32. In addition, text files are generated containing the data results for each element in all sandwich sets allowing for data reduction. In the specific case of the depicted sandwich, the vertical central displacement was 0.17" downward. Also the shear stress on the *XZ* plane appears to be fairly consistent through the thickness of the sandwich core in the areas where shear failure is suspected from the experiment (between the load and

support points). However, no average value is obtained throughout the entire carbon foam core, thus no comparison is made between these results and the average core shear stress calculated from the experimental flexure tests.

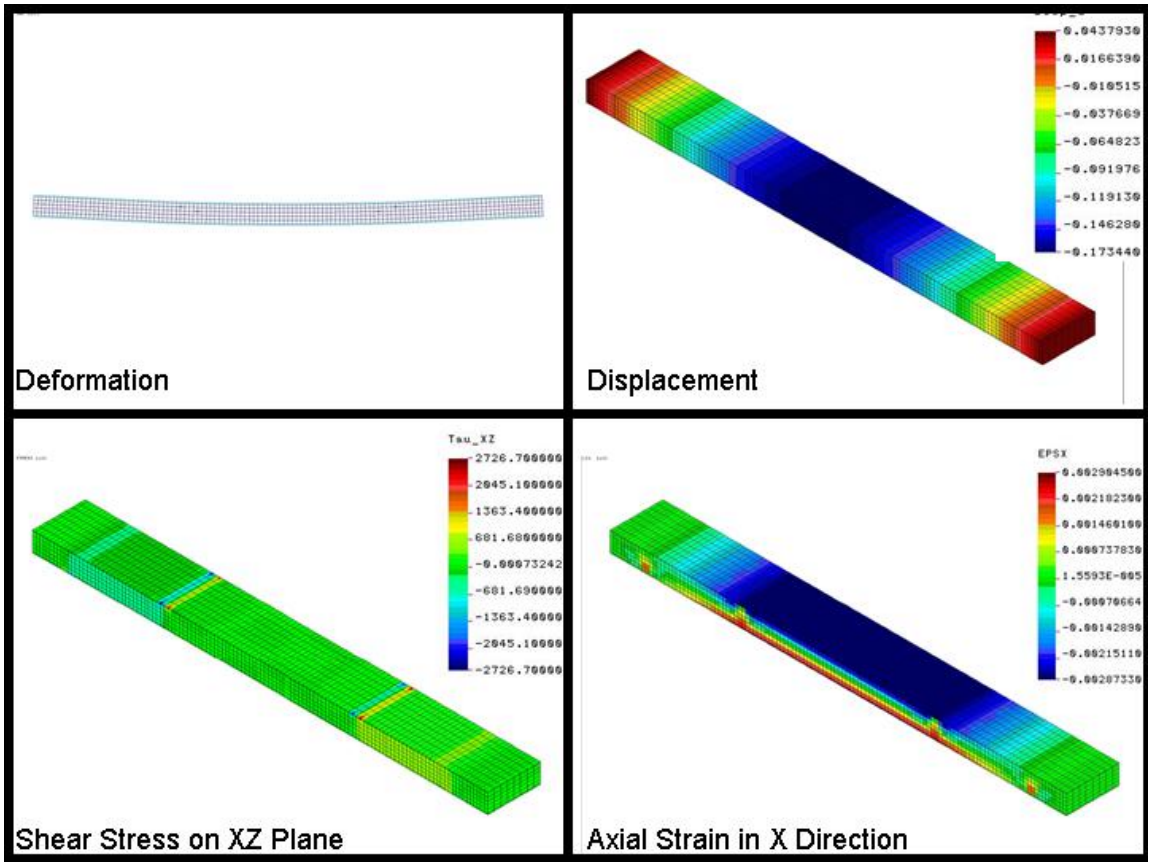

Figure 32. Example FEA plots of deformation, displacement, shear stress and axial strain

The displacement and strain predictions are listed for all sandwich sets in Table 11. In addition, the average experimental results are listed for comparison. Although all the displacements match within 4%, the axial strains on the top face sheet are considerably different from the average recorded experimental values. The difference is attributed to large displacements, and is addressed in section 3.3, where nonlinear

geometric conditions are incorporated by including higher order terms in the strain-displacement relations.

Table 11. Comparison of experimental and linear FEA results

	Displacement [in]			Strain		
	Cosmos	Experimental	Difference [%]	Cosmos	Experimental	Difference [%]
Sandwiches A-E	0.0736	0.071	3.48	2297	2226	3.19
Sandwiches F-K	0.2383	0.238	0.06	3948	2349	68.07
Sandwiches L-P	0.1734	0.171	1.21	2873	2684	7.04
Sandwiches Q-Z	0.1100	0.109	0.77	1823	2386	23.60
Sandwiches P1	0.2429	0.250	2.81	4207	2080	102.26
Sandwiches P2	0.2143	0.221	2.92	3712	1845	101.19

The region of interest is the area between the load and support points where damage initiation was observed during experimentation. The shear stress distribution through the thickness of the sandwich is displayed for each set of sandwiches. These results are presented in Figure 33 for the midpoint between the load and support points. In all cases, the shear stress through the thickness is of the classical distribution. The shear stress does not go to zero at the top and bottom of the sandwich because the value represented at normalized distances 0 and 1 is the average shear stress in the element at the bottom and top of the sandwich, respectively. If the top surface or bottom surface values had been plotted, the values would have gone to zero at these normalized distances.

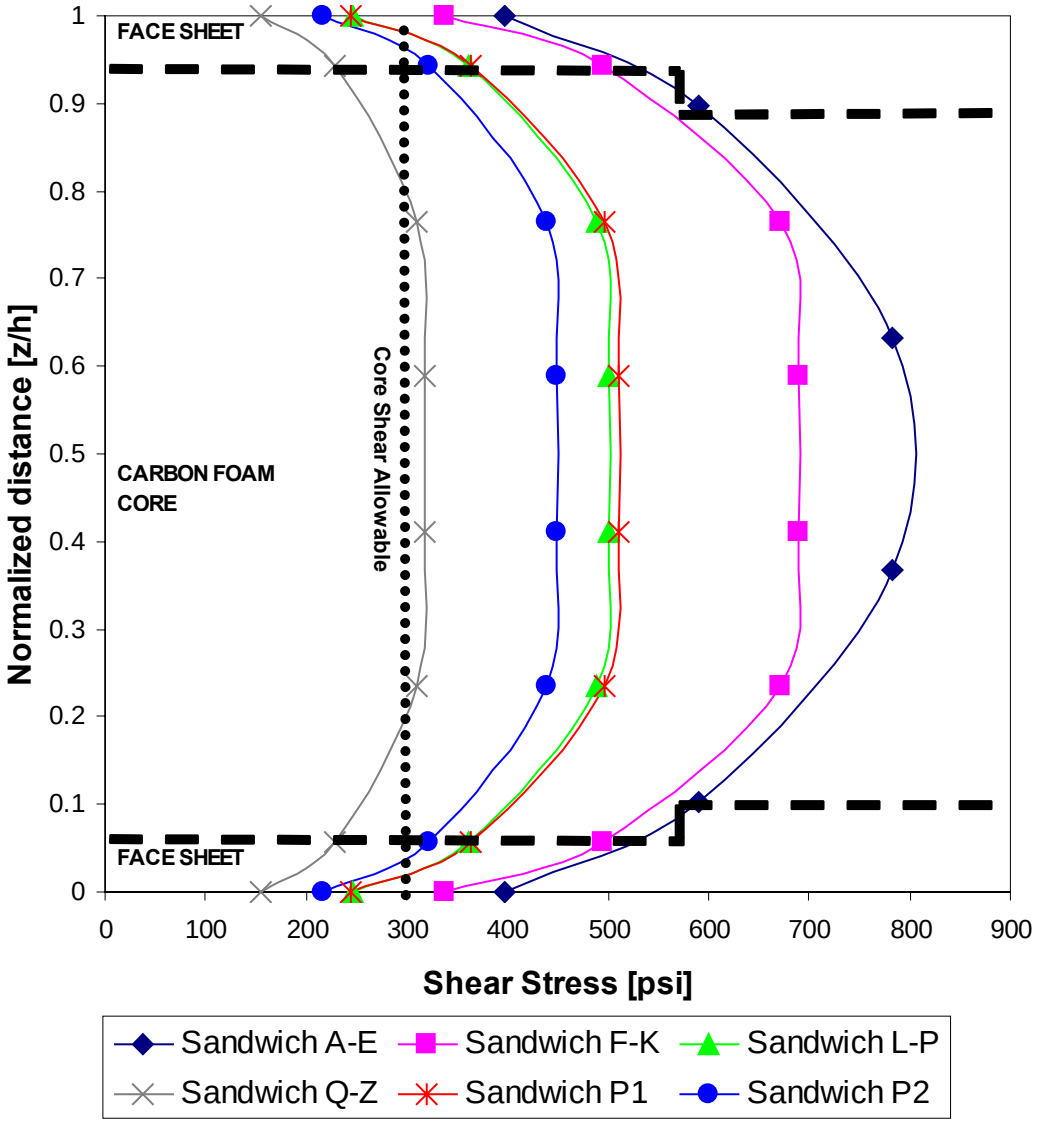

Figure 33. Through the thickness representation of shear stress in the *XZ* plane

Note that the shear strength of the carbon foam provided by the Touchstone Research Laboratory is exceeded in this region. It is however difficult to determine if the failure occurs in the carbon foam core itself or at the bond line. Thus an additional study is undertaken to investigate the bond line stresses and strains as described in section 3.4. In addition, the shear stress tends to flatten in the area of the core indicating

a more constant shear stress in the carbon foam. However, it is difficult to identify a core allowable from these results as the scatter is large and there may be dependence on geometry of the sandwich. In addition, these results are not compared to experimental shear stress values calculated from ASTM C 393 because they represent specific values at a given distance along the length of the sandwich, whereas the ASTM standard gives an average value throughout the core.

3.3 Progressive Damage Flexure Study

In the previous study, discrepancy exists between experimental strain values and predictions. This difference is attributed to the beam undergoing large displacements, thus violating the Kirchhoff hypothesis as stated in section 3.1. In order to account for these large displacements, the three dimensional strain-displacement field in a total Lagrangian formulation is used [29,30].

3.3.1 Material Properties

The apparent laminate properties, from CLPT, of the face sheet lay-up given in Table 3 are used as input into Cosmos M. In addition, a nonlinear elastic behavior is prescribed for the carbon foam core. The initial slope, as seen in Figure 34, is decreased at the critical strain value associated with damage initiation from the experiments to simulate failure. Due to the ligament nature of the carbon foam microstructure, individual ligaments fail during loading. Damage initiation occurs when a critical number of these ligaments have failed, thus softening the carbon foam. However, the carbon foam continues to carry load until complete failure occurs at a later load increment. No data is available to determine the appropriate reduction in properties to accurately model the nature of failure, thus an arbitrary value of 60% reduction is chosen

for this study. Attempts to determine the sensitivity of this value were not undertaken due to time constraints.

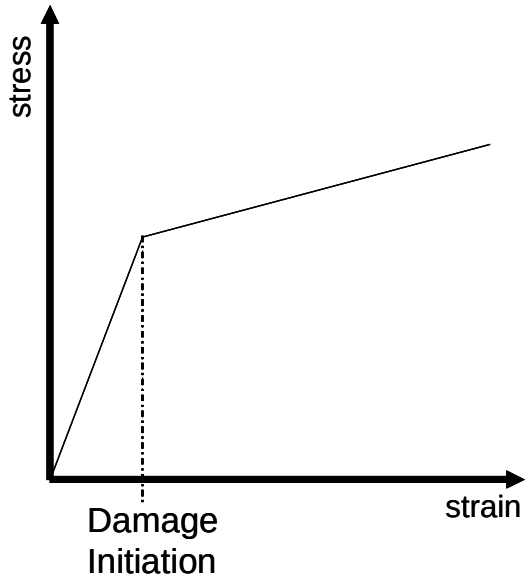

Figure 34. Nonlinear elastic carbon foam core behavior during progressive damage

3.3.2 Boundary Conditions and Loading

The model is restrained and loaded to simulate the four point flexure experiment described in section 2.1. All nodes along two parallel lines on the bottom surface of the bottom face sheet are constrained to prevent translation in the *Y* and *Z* directions. In addition, a single node on one side is restrained from translation in the *X* direction. This method of applying the restraints allows the sandwich beam to slip axially during the loading as seen in Figure 35. Uniform load per unit width is placed on the top face sheet along two parallel lines and is introduced incrementally.

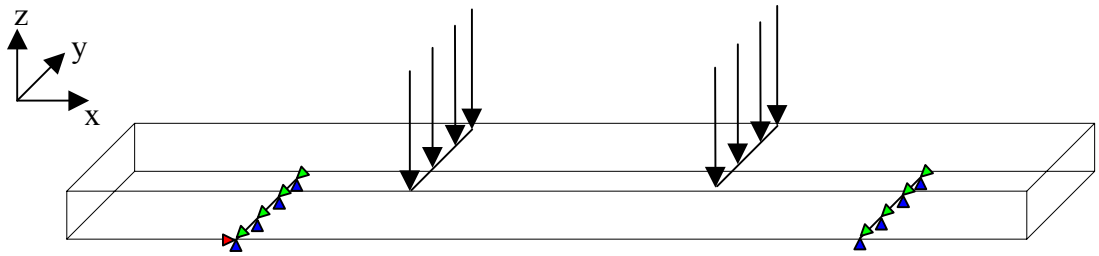

Figure 35. Schematic of progressive damage boundary conditions and loading

3.3.3 Progressive Damage Analysis Results

Plots of deformation, displacement, shear stress and axial strain similar to those presented in section 3.2 are generated, along with text files of data, for each load increment in all sandwich configurations. The displacement and strain predictions for the 0.25" core are listed in Table 12. In addition, the average experimental results have been listed for comparison. The displacements predicted by the progressive damage model are in difference of less than 4% and the strains have a maximum difference of 3.6%. Note that no comparison is made between shear stress values predicted and calculated values from the experimental flexure tests. The shear stress is a function of position along the length of the sandwich, however, in the ASTM C 393 calculations, only the average shear stress throughout the core is calculated.

Table 12. Comparison of progressive damage results for 0.25" core thickness

LOAD		DISPLACMENT				STRAIN		
Increment [lb]		Experimental [in]	Cosmos [in]	% Change		Experimental [μ]	Cosmos [μ]	% Change
50		-0.022	-0.022	0.2%		-684	-688	0.6%
100		-0.044	-0.044	0.2%		-1355	-1381	2.0%
150		-0.066	-0.066	0.5%		-2030	-2077	2.3%
155		-0.068	-0.068	0.5%		-2080	-2147	3.2%
160		-0.070	-0.071	0.5%		-2159	-23217	2.7%
165		-0.073	-0.073	0.7%		-2229	-2286	2.6%
170		-0.075	-0.076	1.3%		-2281	-2356	3.3%
175		-0.077	-0.078	1.9%		-2346	-2425	3.4%
180		-0.079	-0.081	2.5%		-2414	-2495	3.4%
185		-0.081	-0.084	3.1%		-2479	-2565	3.5%
190		-0.083	-0.087	3.8%		-2544	-2635	3.6%

In addition, the load increments and corresponding number of elements that failed during a given increment are listed in Table 13 for the 0.25" core thickness. Recall that an element in considered failed when it has surpassed the critical strain as in Figure 34 and properties are decreased to mimic damage in the core. The average damage initiation load from the experimental flexure experiments is 165 lbs. The progressive damage model indicates that damage initiation occurs at 156 lbs, representing a difference of 5%. The damage progression in the 0.25" core sandwiches is depicted in Figure 36 and shows the traditional shear pattern of failure at 45°.

Table 13. Load increments and corresponding number of failed elements for 0.25” core

INCREMENT	LOAD	# FAILED	% Failed
1	75	0	0%
2	150	0	0%
3	154	0	0%
4	155	0	0%
5	156	2	0%
6	157	2	0%
7	158	9	1%
8	159	16	3%
9	160	36	6%
10	161	66	11%
11	162	125	20%

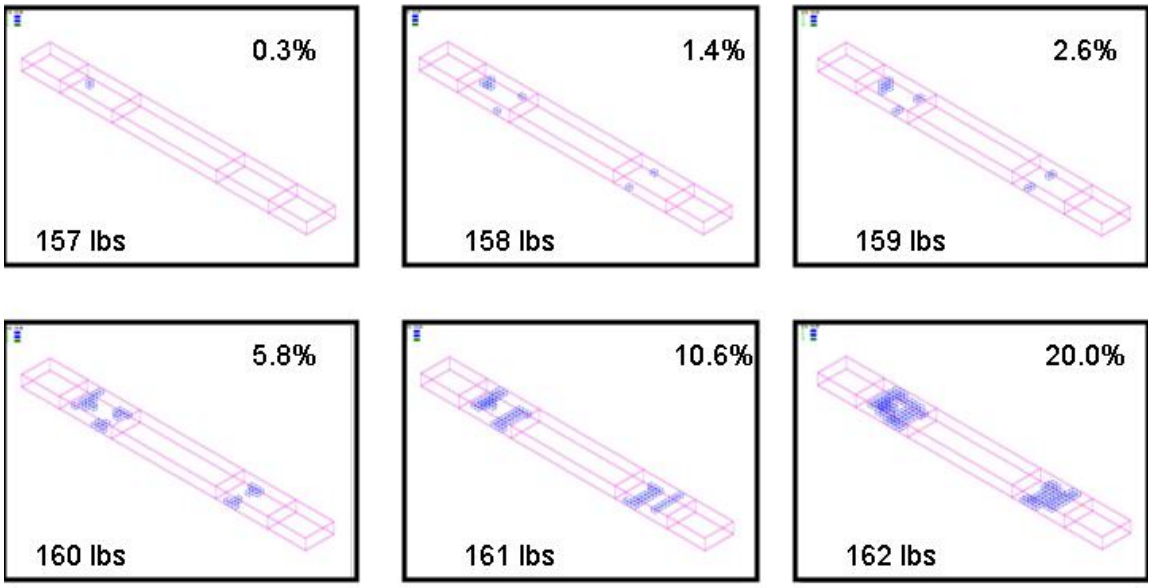

Figure 36. Schematic of damage progression in 0.25” core

The progressive damage results for the 0.5” core is listed in Table 14. In addition the average displacements and strains from the experimental study are listed. The displacements predicted by the progressive damage model are in difference of less than

1.3% and the strains have a maximum difference of 7%. Again, the shear stress values are not compared to experimental results for reason stated previously.

Table 14. Comparison of progressive damage results for 0.5" core thickness

LOAD	DISPLACMENT			STRAIN		
Increment [lb]	Experimental [in]	Cosmos [in]	% Change	Experimental [μ]	Cosmos [μ]	% Change
400	-0.173	-0.171	1.2%	-2178	-2121	2.6%
450	-0.195	-0.192	1.2%	-2488	-2387	4.0%
475	-0.206	-0.204	0.9%	-2712	-2524	6.9%
500	-0.216	-0.216	0.4%	-2775	-2659	4.2%
520	-0.225	-0.225	0.2%	-2810	-2767	1.5%
540	-0.234	-0.235	0.7%	-2915	-2875	1.4%
560	-0.242	-0.245	1.1%	-2812	-2984	6.1%

The load increments and element failure for the 0.5" core thickness are listed in Table 15. Recall that the average damage initiation load during experimentation is 380 lbs. The progressive damage model indicates damage initiation at 400 lbs, a difference of 5%.

Table 15. Load increments and corresponding failed elements for 0.5" core

INCREMENT	LOAD	# FAILED	% Failed
1	150	0	0%
2	300	0	0%
3	400	4	1%
4	450	8	1%
5	475	11	2%
6	500	24	4%
7	520	36	6%
8	540	56	9%
9	560	68	11%
10	580	92	15%
11	600	190	30%

The damage progression in the 0.5” core sandwiches is depicted in Figure 37. In addition, the core shear zone on the right end has been enlarged to show the failure progression in detail in Figure 38. The initial failed elements are likely due to edge effects in the sandwich. Then the entire row of elements along the top surface of the core near the loading line fails, in the same manner as the damage initiation crack formed during the experiment. Note that the failure develops in a traditional shear pattern at 45°.

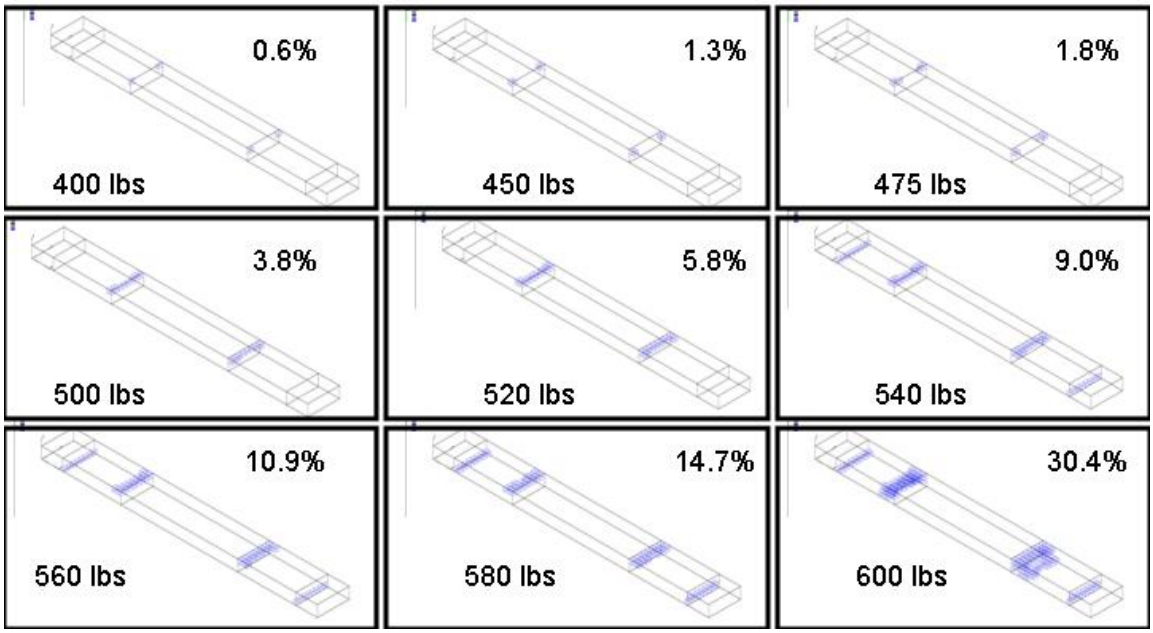

Figure 37. Schematic of damage progression in 0.5” core

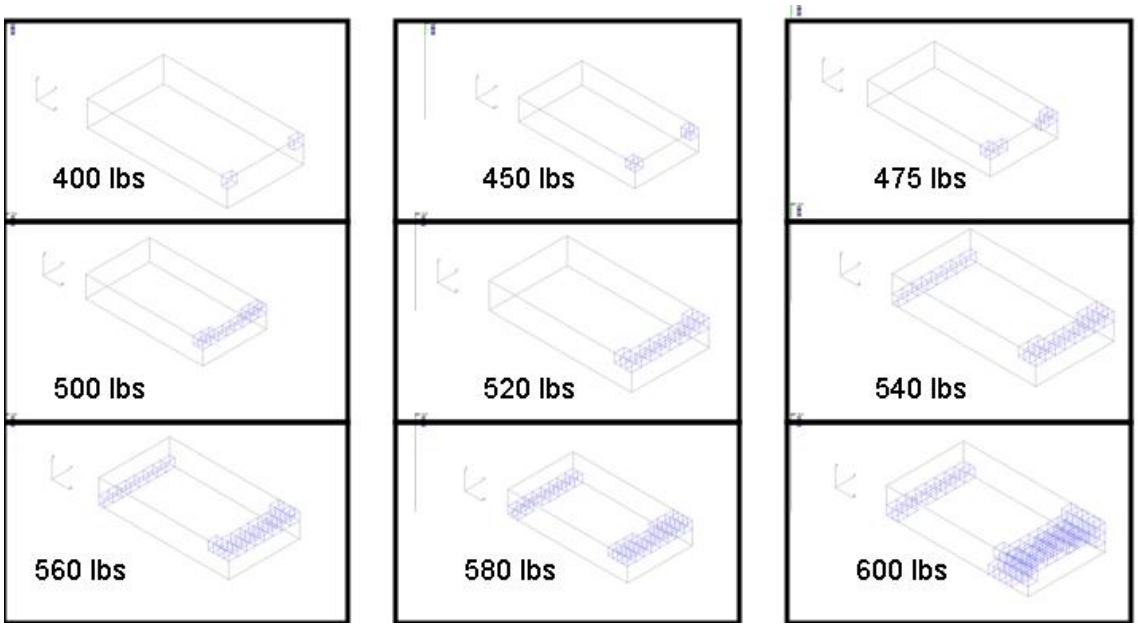

Figure 38. Enlarged damage progression in 0.5” core in right shear zone

3.4 Bond Line (Interface) Study

A bond line study is undertaken to determine the source of damage initiation in the sandwich beams. A 15 mil bond line is introduced with 5 mils of pure adhesive and a 10 mil “wicking” region as in Figure 39. This "wicking" region occurs due to the porous nature of the carbon foam, which allows the adhesive to penetrate the surface resulting in a layer of carbon foam plus adhesive. The computational phase of this study is conducted with a commercial software package, Stress Check [31].

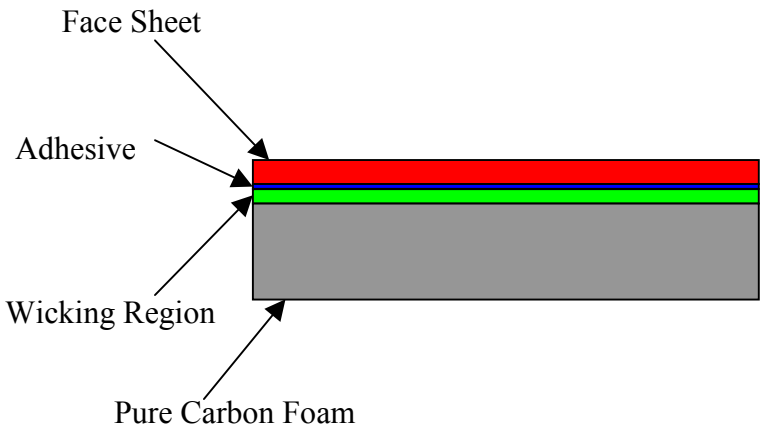

Figure 39. Schematic of bond line layers

The model is discretized such that it is possible to study the stresses and strains in the layers next to the bond line. This involves modeling one layer for each of the following—the entire face sheet, the adhesive, and the wicking region. The core is treated as two layers in order to get closer to the aspect ratios of the adjacent layers. The total number of elements across the length of the model is eight, with only a single element used across the width. The model mesh consists of 8 node brick elements with linear, elastic material properties.

3.4.1 Material Properties

The material properties for the bond line study are presented in Table 16. Material properties for the carbon foam, face sheet materials and adhesive are obtained from manufacturer's data. The only exception is for the shear strength of the adhesive, which is estimated as one-half of its tensile strength. A simple rule of mixtures is applied to find the effective material properties of the wicking region by assuming a volume fraction of 75% carbon foam, derived from the porosity value. Also note that for this analysis, apparent properties of the face sheet are not used. Rather, Stress Check

allows the user to input the ply stacking sequence of the face sheets and constituent material properties and calculates its own effective properties.

Table 16. Material properties for bond line analysis

Face Sheets	**E1**	**E2**	**NU12**	**G12**
Plain Weave	1.02E+07	1.02E+07	0.3	2.03E+06
Uni-Tape	2.63E+07	1.49E+06	0.28	1.04E+06
Adhesive	**E1**	**E2**	**NU12**	**G12**
105/205	4.08E+05		0.3	
Core	**E1**	**E2**	**NU12**	**G12**
Carbon Foam	1.50E+05		0.35	4.90E+04
Wicking Region	**E1**	**E2**	**NU12**	**G12**
Foam+Adhesive	2.15E+05		0.34	

The strength of the wicking material system is estimated as the average of the strength of the core and adhesive independently, weighted with the volume fractions of each constituent. It is assumed that this region will be stronger than the core, but weaker than the adhesive.

3.4.2 Boundary Conditions and Loading

The model is constrained along two lines parallel to the width of the sandwich as seen in Figure 40. Translation in the *Z* and *Y* direction is prevented, while the sandwich is allowed to slip in the *X* direction. A condition of symmetry is also shown in Figure 40 so that only the left-hand side has to be modeled. In addition, the overhang region at either end of the sandwich is not modeled since it is not an area of interest in the bond line study.

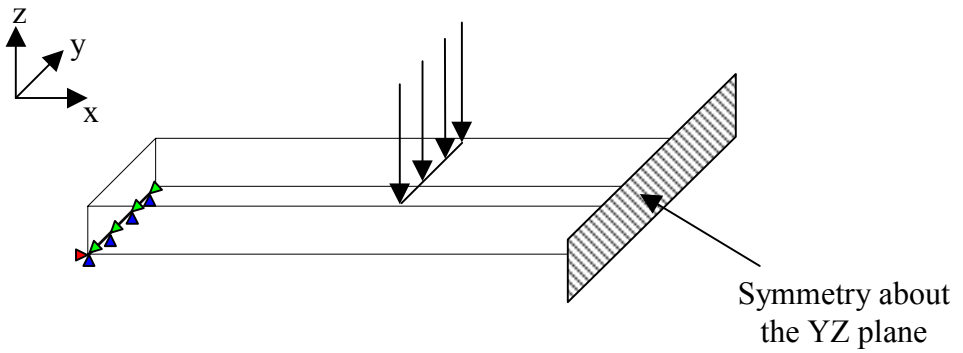

Figure 40. Schematic of bond line boundary conditions and loading

Representative sets of sandwiches are modeled to investigate the dependency of the two core thicknesses, namely set A-E and set F-K. The average loads recorded at the onset of damage during experimentation is applied to the models as a uniform load per unit length along a line across the width of the top face sheet as shown in Figure 40. Linear displacements and elastic material properties are assumed in this model.

Stress Check employs a p-value scheme instead of the traditional h-value scheme for mesh refinement. In the h-version, the mesh is refined by subdividing existing element into smaller elements of the same type [32]. In p-version, the same mesh size is used, but the existing elements are replaced by elements of higher order, i.e. quadratic versus linear. The bond line models are analyzed with p-values of 1 through 8.

3.4.3 Bond Line (Interface) Study Results

Several plots are generated for each set of sandwich specimens. Examples of the displacement, shear stress and axial strain plots appear in Figure 41. Notice that

particular elements can be examined alone to determine the shear stress or strain distribution within the element.

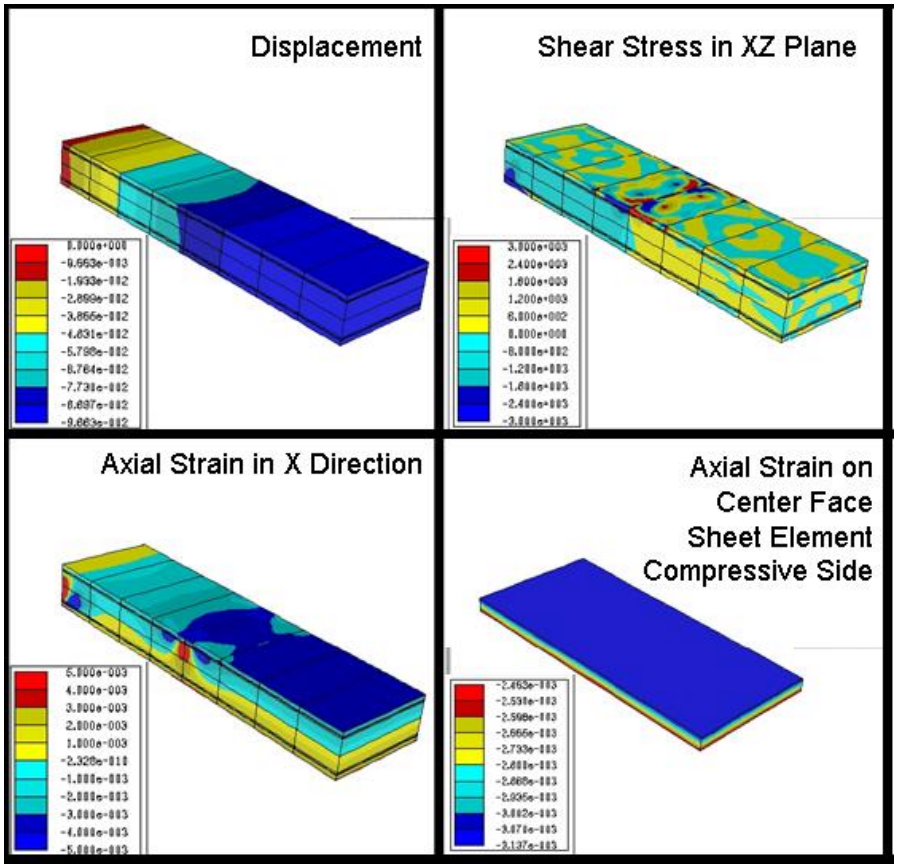

Figure 41. Example bond line study output from Stress Check

The average experimental data and the computational results from Stress Check are summarized in Table 17. For beams with 0.25" cores, the computational displacement results match within 1.4% of the average experimental values. For the 0.5" core beams, the displacement predictions are within 1% of the average experimental results.

Table 17. Comparison of average experimental and computational bond line results

	0.25" Core Thickness		
	Experimental	**Computational**	**Difference [%]**
Applied Load [lb]	165.39	165.39	--
Axial Strain [μ]	2226	3137	40.93
Vertical Displacement [in]	0.0953	0.0966	1.38
	0.5" Core Thickness		
	Experimental	**Computational**	**Difference [%]**
Applied Load [lb]	542.64	542.64	--
Axial Strain [μ]	2349	5222	122.31
Vertical Displacement [in]	0.326	0.326	0.03

Although some discrepancies may exist due to large displacements as previously described, it is assumed that the model is valid for predicting the behavior of a carbon foam sandwich beams under flexure loading since the displacements match very closely for both core sizes. While the strain levels do not match as closely, there is still enough evidence to determine the location of damage initiation.

Plots of the shear stress distribution at the bond line are generated as in Figure 42 to determine the stresses at each layer of the bond line. Data output is obtained for average values at given point in bond line for analysis of source of damage initiation. These values can not be compared to experimental shear stress results in the core because during the experiment only the average shear stress throughout the entire core was calculated. The predicted shear stress results are for a given area of the core, not an overall average throughout.

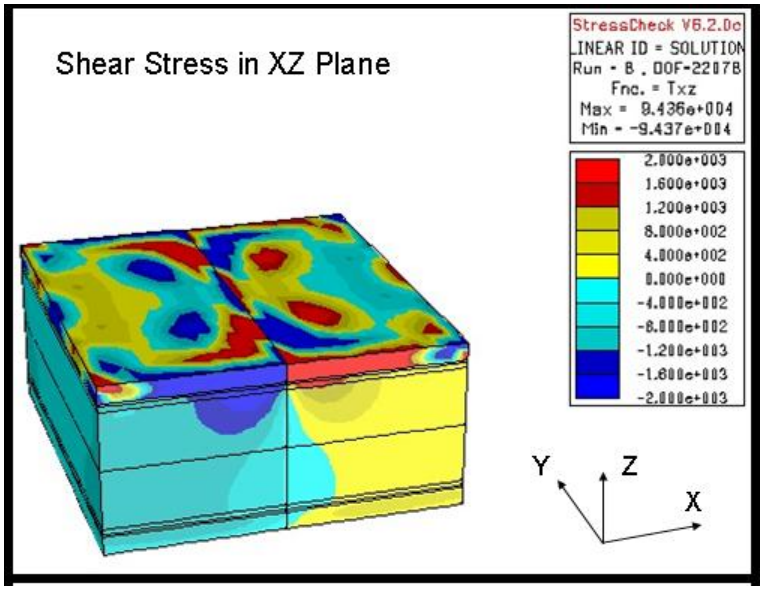

Figure 42. Shear stress distribution at bond line

The computational shear stress values and respective strengths for the bond line area are summarized in Table 18. Recall that the wicking material system strength is a weighted average of the adhesive and carbon foam strengths. For both core sizes, more than one layer of the bond line appears to fail in shear; however, the stress to strength ratio in the carbon foam core is largest in both core sizes. In addition, after testing, the delaminated face sheets remain rough in texture. This roughness dimension well exceeds the wicking region thickness. These two observations indicate that, although other layers may be undergoing damage at this load level, the carbon foam core is the most likely source for damage initiation.

Table 18. Comparison of shear stress and material strength at the bond line

	0.25" Core Thickness			
	Shear Stress	**Shear Strength**	**Stress/Strength Ratio**	**Failure ?**
Adhesive	3500	~4000	0.88	NO
Wicking Region	2700	~2000	1.35	YES
Core	2000	300	6.67	YES
	0.5" Core Thickness			
	Shear Stress	**Shear Strength**	**Stress/Strength Ratio**	**Failure ?**
Adhesive	7900	~4000	1.98	YES
Wicking Region	5000	~2000	2.50	YES
Core	4000	300	13.33	YES

4. CONCLUSIONS

As an emerging material system, carbon and graphite foams have great potential in various industries encompassing aerospace, military, offshore, power production and other commercial industries for applications like radiators, advanced power electronic heat sinks, fireproof containers, "elevator" floor for aircraft carriers, lightweight ship hulls, EMI and radar-selective shielding.

In the present study, overall flexure response and material properties are explored through an integrated experimental and computational approach. Specifically, mechanical properties and failure modes of sandwich beams with carbon/epoxy laminate face sheets and carbon foam core are characterized.

The ASTM C 393 flexure tests reveal that the dominant failure mode is shear in the carbon foam core. Even though delamination is observed in the experiments, it did not occur at the face sheet/core interface, and subsequent computational studies support this fact. The beam bending stiffness is found as 6,340 lb-in^2 for the 0.25" core and 41,687 lb-in^2 for the 0.5" core thickness. In addition, a critical damage initiation strain is identified as 2,268 με, measured in the axial direction along the length of the sandwich beams on the compressive face sheet.

Tensile and shear experiments are conducted according to ASTM standards on the carbon foam specimens. Specimens with straight edges are used in the ASTM C 297 tensile experiment, and the elastic modulus is evaluated as 39 ksi. ASTM C 1292 experiments with Iosipescu shear specimens revealed an average shear modulus of 21 ksi. The carbon foam core was considered isotropic indicating that shear modulus (G) and Young's modulus (E) are related through the Poisson's ratio. These values produce a Poisson's ratio of -0.0714, however, it is important to note that the Young's modulus had a standard deviation of 8.25 ksi and the shear modulus had a standard deviation of 8 ksi. Thus the actual Poisson's ratio could range from -0.3275 to 0.5 indicating that more experimental work is required to resolve the Poisson's ratio of carbon foam.

In addition to the experimental methods, computational models are developed to further investigate flexure response and associated damage mechanisms in the sandwich beams. The initial analysis is based on the classical laminated plate theory (CLPT) wherein the sandwich beam is represented as a laminate of individual plies of the face sheets and several plies of carbon foam. The corresponding results clearly display the shortcomings of CLPT assumption in predicting strain fields for this material system and geometry.

Thus, a series of detailed FEA models are developed to assess the flexural response as observed in the experiments. Initially, small displacements and linear elastic constitutive material models are formulated. The face sheets are represented by a single layer, with homogenized orthotropic properties and the carbon foam core is considered isotropic. Even though the displacements matched the experimental data, the strain field does not. However, when total Lagrangian formulation is implemented to account for large displacements, both strain and displacement predictions match the experimental results. In addition, a progressive damage study is conducted by implementing a strain criterion, identified from experiments, for the carbon foam core and the corresponding flexural response match the testing results very well.

An additional study of the bond line, or interface between the core and the face sheet, reveals that the delamination is confined to the interior of the core and is not inside the bond line. This finding is supported by the flexure experiments, where the face sheets had a rough foam surface still adhered to them. The multifaceted results of the research, i.e. identification of a dominate damage mechanism as shear in the core, experimentally capturing critical strain at damage initiation and development of efficient FEA models to predict flexural response, have provided valuable insight and encouragement to seriously consider carbon foam core sandwich components in structural applications.

REFERENCES

1. Touchstone Research Laboratory. CFOAM Super-Carbon Foam. 2001. http://www.cfoam.com. Accessed June 2002.
2. Li, K., Gao, X.-L., and Roy, A.K. (2003). Micromechanics model for three-dimensional open-cell foams using a tetrakaidecadhedral unit cell and Castigliano's second theorem. *Composite Science and Technology*, **63**: 1769-1781.
3. Gallego, N. and Klett, J. (2003). Carbon foams for thermal management. *Carbon*, **41**: 1461-1466.
4. Krause, C. (2000). ORNL's graphite foam may aid transportation. *Oak Ridge National Laboratory Review*, **33**:26-27.
5. Oak Ridge National Laboratory Carbon Materials Technology Group. High Thermal Conductivity Graphite Foams. http://www.ms.ornl.gov/researchgroups/cmt/foam/foams.htm. Accessed August 2003.
6. Brown, M. and Crane, R. (2002). Development of carbon foam for naval structures. In: *Proceedings of the Society of Allied Weight Engineers, Inc.*, May 20-22, 2002.
7. Griffith, G. (2002). Carbon foam: a next-generation structural material. *Industrial Heating*, **v69(11)**: 47-52.
8. Navy CAP Virtual Showcase. Touchstone Research Laboratory. http://www.navysbir.brtrc.com/cap/briefingsadmin/ts.asp. Accessed September 2003.
9. WVHTF. Touchstone's Carbon Foam to Fly. http://www.wvhtf.org/mag/v5n6/touchstone.htm. Accessed June 2002.
10. Callister, W. D. (2000). *Material Science and Engineering: An Introduction*. 5th Edition. John Wiley & Sons, Inc, New York.

11. Zenkert, D. (1995). *An Introduction to Sandwich Construction.* Chameleon Press Ltd., London..
12. Davies, P. and L., Lionel. Preliminary structural design of sandwich cored vessels. *Nautical Construction with Composite Materials. International Conference*, Paris. December 7-9, 1992.
13. Gibson, L.J. and Ashby M.F. (1997). *Cellular solids: structures and properties*. 2nd Edition. Cambridge University Press, Cambridge.
14. Sihn, S. and Roy, A.K. (2001). Modeling and stress analysis of open-cell carbon foam. *46th International SAMPE Symposium*, May 6-10, 2001.
15. Kanaun, S.K. and Kochekseraii, S. B. (2003). A numerical method for the solution of thermo- and electro-static problems for a medium with isolated inclusions. *Journal of Computational Physics*, http://www.sciencedirect.com.
16. Meraghni, F., Desrumaux, F. and Benzeggragh, M.L. (1999). Mechanical behavior of cellular core for structural sandwich panels. *Composites: Part A*, **30**: 767-779.
17. Triantafillou, T.C. and Gibson, L.J. (1987). Failure mode maps for foam core sandwich beams. *Material Science and Engineering*, **95**: 37-53.
18. Dai, J. and Hahn, H. (2003). Flexural behavior of sandwich beams fabricated by vacuum-assisted resin transfer molding. *Composite Structures*, **61**: 247-253.
19. Sokolinsky, V., Shen, H., Vaikhasnski, L. and Nutt, S. (2003). Experimental and analytical study of nonlinear bending response of sandwich beams. *Composite Structures*, **60**: 219-229.
20. Hall, R. and Hager, J. (1996). Performance limits for stiffness-critical graphitic foam structures. Part I: Comparisons with high-modulus foams, refractory alloys and graphite epoxy composites. *Composites Materials*, **30**: 1922-1937.
21. Hall, R. (1996). Performance limits for stiffness-critical graphitic foam structures. Part II: Comparisons of foams, foam-core and honeycomb-core sandwiches in bending/shear. *Composites Materials*, **30**: 1938-1956.

22. Standard Test Method for Flexural Properties of Sandwich Constructions. *Annual Book of ASTM Standards*. Volume 15.03. ASTM C 393-001.
23. West System. Epoxies. http://www.westsystem.com. Accessed April 2003.
24. Standard Test Method for Flatwise Tensile Strength of Sandwich Constructions. *Annual Book of ASTM Standards*. Volume 15.03. ASTM C 297-94.
25. Standard Test Method for Shear Strength of Continuous Fiber-Reinforced Advanced Ceramics at Ambient Temperatures. *Annual Book of ASTM Standards*. Volume 15.01. ASTM C 1292-00.
26. Daniel, I.M and Ishai, O. (1994). *Engineering Mechanics of Composite Materials.* Oxford University Press, Inc., New York.
27. The Laminator: Classical Analysis of Composite Laminates. http//www.thelaminator.net. Accessed August 2002.
28. Structural Research and Analysis Corporation. Cosmos. http://www.cosmosm.com. Accessed August 2003.
29. Slaughter, W. (2002). *The Linearized Theory of Elasticity*. Birkhäuser, Boston.
30. Cook, R. (1981). *Concepts and Applications of Finite Element Analysis.* 2nd Edition. John Wiley & Sons, New York.
31. Engineering Software Research and Development. Stress Check. http://www.esrd.com. Accessed April 2003.
32. Reddy, J.N. (1993). *An Introduction to the Finite Element Method.* 2nd Edition. McGraw-Hill, Inc., Boston.

VITA

Melanie Diane Sarzynski was born to Michael and Teresa Sarzynski in Amarillo, Texas, on August 8, 1980. She attended Amarillo High School in Amarillo and upon completion in 1998 entered the Department of Mechanical Engineering at Texas A&M University. She completed a two term co-op assignment with the DFAB Yield Enhancement group at Texas Instruments in Dallas, Texas. In the summer of 2002, she began research with Dr. Ozden Ochoa through the Undergraduate Research Program. Upon completion of her Bachelor of Science degree in December 2002, she began work on her Master of Science degree in Mechanical Engineering. In the spring of 2002, she received honorable mention in the NSF Graduate Research Fellowship competition and in December 2003 she completed her Master's degree. Melanie can be reached at 3508 Carlton, Amarillo, TX 79109.